Hot orogen behaviour, partial melting and ductile flow: Case study of the Damara Orogen, Namibia

Authors: Thomas Lloyd Jones[1,2], Klaus-Peter Knupp[3], Alex Otto[4], Ed Becker[4,5], Andy Wilde[6]

Corresponding author: tl.jonesy8@gmail.com

1) School of Geosciences, University of the Witwatersrand, Johannesburg, South Africa.
2) TLJ Structural Geology Consulting Ltd, Edinburgh, UK
3) Earthmaps Consulting, Swakopmund, Namibia
4) Deep Yellow Ltd, Subiaco, Western Australia
5) Marc Geology Pty Ltd, Hillarys, Western Australia
6) Boss Energy, 1/420 Hay Street, Subiaco, WA 6010, Western Australia

Key points:

1) The Damara Orogen preserves the first-order architecture of a hot collisional orogen.
2) A two-stage magmatic evolution is consistent with the timeframe required for radiogenic heating and progressive thermal weakening.
3) Partial melting fundamentally changed deformation style, leading to distributed ductile flow in the Central Zone.

This is a non-peer reviewed preprint submitted to EarthArXiv.

This preprint has been submitted to review at *Tectoncis.*

Abstract

The Damara Orogen in Namibia preserves an exceptional record of Neoproterozoic–Cambrian continent–continent collision during Gondwana assembly. It provides a natural laboratory suitable for testing thermomechanical models of hot orogens. We integrate regional-scale structural mapping from satellite imagery and aeromagnetic data with published lithostratigraphic, metamorphic, magmatic, and geochronological constraints; this is used to evaluate the first-order architecture and tectonic evolution of the belt. Results show strong partitioning between a high-temperature, low-pressure (HTLP) Central Zone and lower-temperature, higher-pressure (LTHP) Northern and Southern zones. The Central Zone is characterised by Buchan-series metamorphism, widespread granite–migmatite terranes, voluminous crustally derived leucogranites, complex dome-and-basin interference patterns, non-cylindrical folds, and distributed syn-magmatic deformation. In contrast, the flanking zones preserve comparatively linear fabrics, inverted Barrovian metamorphic gradients, and foreland-vergent fold-and-thrust architectures consistent with oppositely dipping marginal wedges. Igneous evolution in the Central Zone records early calc-alkaline to tholeiitic magmatism at ca. 575–540 Ma, followed by widespread crustal-melt leucogranite magmatism at ca. 530–510 Ma; this 2-stage time-evolution is characteristic of radiogenic heat production in thickened crust. We interpret the Damara Belt as a hot orogen in which partial melting triggered a transition from wedge-dominated contractional tectonics to distributed mid-crustal flow within the Central Zone. The Damara Orogen demonstrates how temperature, partial melting, and crustal rheology fundamentally influence deformation during continental collision. It further demonstrates that even moderately sized orogens may evolve large-hot-orogen style behaviour under favourable thermal conditions.

1) Introduction

The evolution of continental collision zones is a central problem in tectonics, since orogens record the processes by which continents grow, crust thickens, melts are generated, and lithosphere is mechanically reorganised and chemically differentiated. Ancient collisional belts complement active systems by exposing deeper crustal levels and preserving the long-term products of deformation, metamorphism, and magmatism. Comparisons between exhumed ancient orogens and active belts such as the Himalayan–Tibetan system offer an important means of testing geodynamic models across a range of spatial and temporal scales throughout different geological eras.

The architecture of collisional orogens varies between systems. Some orogens are dominated by relatively cool, frictional upper-crustal wedges expressed as fold-and-thrust belts and accretionary prisms (e.g., Westbrook et al., 1988; Beaumont et al., 2000; Steck, 2008). Meanwhile, other orogens contain broad domains of high-temperature metamorphism, crustal melting, granitoid magmatism, and distributed ductile deformation (e.g., Fossen et al., 2017). Numerical and conceptual models suggest that these differences reflect first-order thermal controls on orogen mechanics, encapsulated by thermomechanical models of "hot orogens" (e.g., Jamieson and Beaumont, 2013).

Thermomechanical models of hot orogenic belts are effectively summarised in the conceptual model of Jamieson and Beaumont (2013) (Figure 1). Orogens are believed to originate as small-cold orogens above subduction zones, and in forearcs or early stage continent-continent collision with only minor arc magmatism. The first-order architecture of small-cold orogens consists of single or back-to-back bivergenet critical wedges (e.g. Willett et al., 1993). Deformation is dominated by contractional critical wedge mechanics in accretionary prisms and in the foreland fold-and-thrust belts (Dahlen, 1990; Buiter, 2012). As material is accreted during subduction and collision, orogens may grow along a temperature-magnitude spectrum and evolve into a large-hot orogen (Figure 1; Jamieson and Beaumont, 2013). The transition to a large hot orogen is associated with widespread partial melting under high temperature metamorphic conditions (e.g. Godin et al., 2006; Searle et al., 2009). Partial melting can fundamentally alter the rheology of the crust (Rosenburg and Handy, 2005; Jamieson et al., 2011), meaning widespread migmatite terrains may be dominated by *en-masse* ductile flow in response to differential pressure gradients (Beaumont et al., 2001; Jamieson and Beaumont, 2013). This is supported by geological studies of exhumed migmatite terrains (e.g., Searle et al., 2003; Godin et al., 2006; Chardon et al., 2011; Kruckenberg et al., 2011; Wang et al., 2021), and by geophysical surveys of the present-day Himalaya-Tibet orogen (e.g., Nelson et al., 1996; Clark and Royden, 2000; Unsworth et al., 2005; Royden et al., 2008). Geological and geophysical observations, supported by numerical simulations, present considerable evidence that temperature exerts a

fundamental first-order control on the architecture of collisional orogenic belts (Figure 1; Jamieson and Beaumont et al., 2013).

In this study, we focus on the Neoproterozoic–Cambrian Damara Orogen in Namibia. We integrate new regional structural mapping derived from satellite imagery and aeromagnetic data, alongside published lithostratigraphic, metamorphic, magmatic, and geochronological constraints, to reassess the first-order architecture of the Damara Orogen. We test whether the Damara Belt records the hallmarks of a hot collisional orogen, evaluate the controls on deformation style across the belt, and examine the role of partial melting in facilitating mid-crustal flow. More broadly, we use the Damara Orogen as a natural laboratory to assess how temperature, melt fraction, and rheological heterogeneity govern the mechanical evolution of continental collision zones.

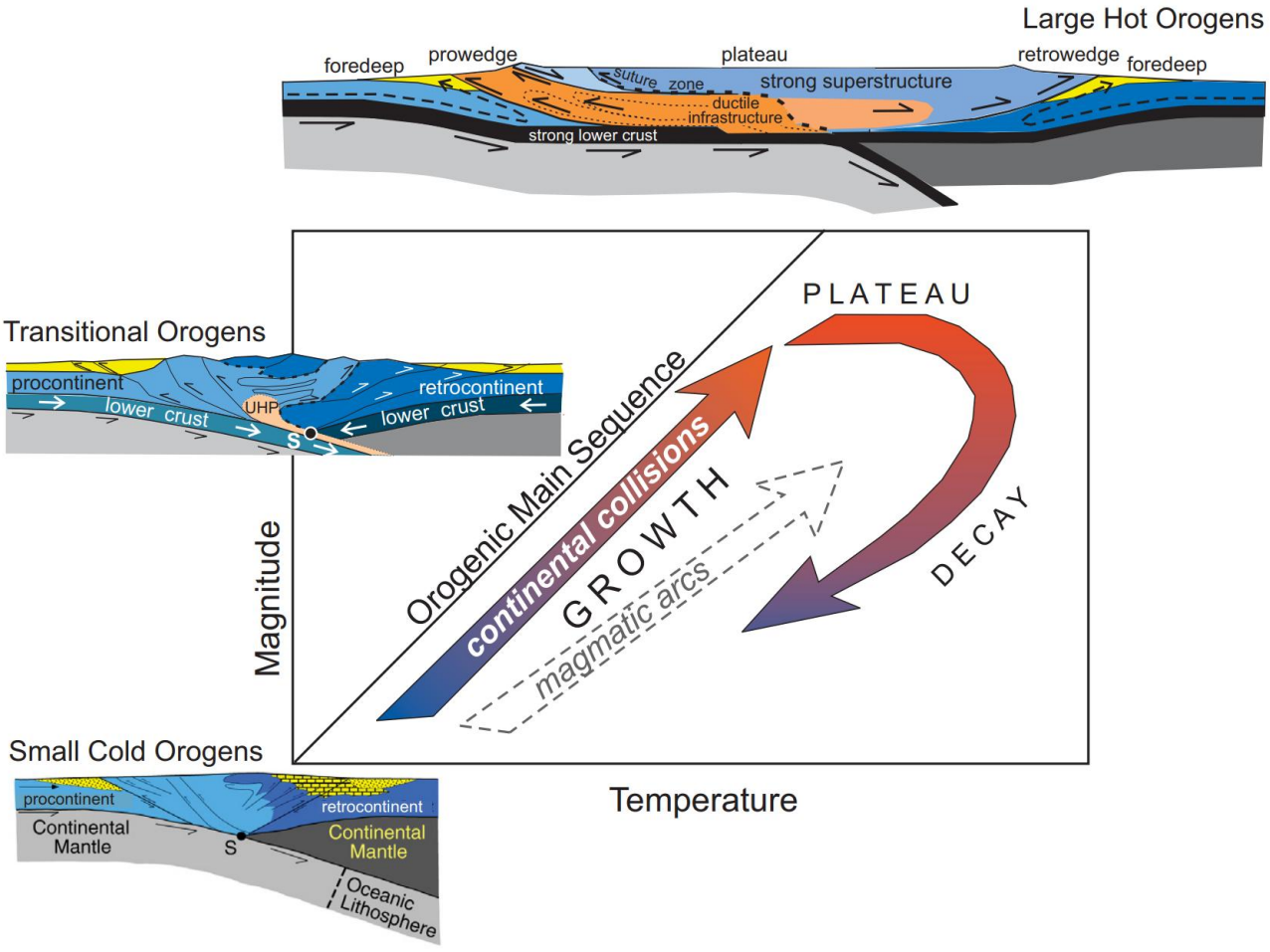

Figure 1 – Conceptual temperature-magnitude diagram showing growth from small-cold to large-hot orogens (after Beaumont et al., 2006 and Jamieson and Beaumont, 2013).

2) Datasets & Methods

Structural fabric mapping was undertaken at the belt-scale using a combination of ASTER satellite data, web-based satellite imagery (Bing and Google), and published geological maps, including the 1:500,000 map of the Damara Orogen by Miller and Grote (1988) and the Geological Survey of Namibia 1:250,000 map series. Pre-processed ASTER datasets were provided by Reptile Mineral Resources and Deep Yellow Ltd.

Aeromagnetic data were integrated with these datasets for more complete structural mapping of the southern Central Zone, including areas concealed beneath superficial cover. The dataset comprised single-sensor total magnetic intensity data acquired on behalf of the Geological Survey of Namibia at 200 m line spacing. Processing included 3D Euler deconvolution, analytic signal, tilt derivative, automatic gain control, total horizontal gradient, horizontal gradient of the tilt derivative, reduction to pole, and first vertical derivative transformations.

A belt-scale synthesis of the lithostratigraphic, metamorphic, and magmatic architecture, together with a compilation of igneous rock age data from the Central Zone, was developed from published literature and unpublished MSc and PhD theses.

3) Geodynamic setting of the Damara Orogen & assembly of Gondwana

The present-day African continent is a collage of continental cratons amalgamated during the Pan-African Orogeny. This culminated in the assembly of the supercontinent Gondwana at c. 500 Ma, as recorded by a wider network of Neoproterozoic orogenic belts stretching across Africa, South America, Australia, and Antarctica (Figure 2; Merdith et al., 2017).

The Damara Belt is associated with an orogenic "triple junction" in western and central Namibia. This records near-simultaneous collision between three different cratons during the amalgamation of Gondwana: 1) The Kaoko Belt records east-west directed collision between the Rio de la Plata and Congo cratons at c. 580-550 Ma (Goscombe et al., 2017a), 2) the Gariep Belt records transpressional deformation and fold-and-thrust belt formation at c. 550 Ma (Frimmel, 2018), and 3) the Damara Belt records northwest-southeast directed collision between the Congo and Kalahari cratons at c. 575-500 Ma (Figure 2).

The Damara Belt is believed to extend northeastwards from Namibia, continuing beneath cover sediments of the Kalahari Desert to merge with the Lufilian Arc and Zambezi Belt in the Democratic Republic of the Congo, southern Zambia, and northern Zimbabwe. This has led to the collective term "Damara-Lufilian-Zambezi belt" (e.g., Merdith et al., 2017) (Figure 2). The eastward extension of the Damara Belt into the Lufilian Arc and Zambezi Belt is significant, as high-pressure eclogites in the Zambezi Belt record evidence for peak pressures of 26-28 kbar at 595+/-10 Ma, 607+/-14 Ma, and 659+/-14 Ma (John et al., 2003, 2004). Based on a low calculated geothermal gradient (~8 ^{O}C/km), combined with the deep subduction required to form pressures of 26-28 kbar, John et al. (2003) estimated that the oceanic domain between the Congo and Kalahari cratons was likely to have been >1000 km wide in its eastern portion. The tectonic style varies greatly along the Damara-Lufilian-Zambezi Belt, with high-temperature and low-pressure conditions in the Damara Belt giving way to low-temperature but high/ultra-high-pressure metamorphism further east in the Zambezi Belt (Goscombe et al., 2020). High-pressure eclogites have not been recognised in the Damara Belt itself in Namibia.

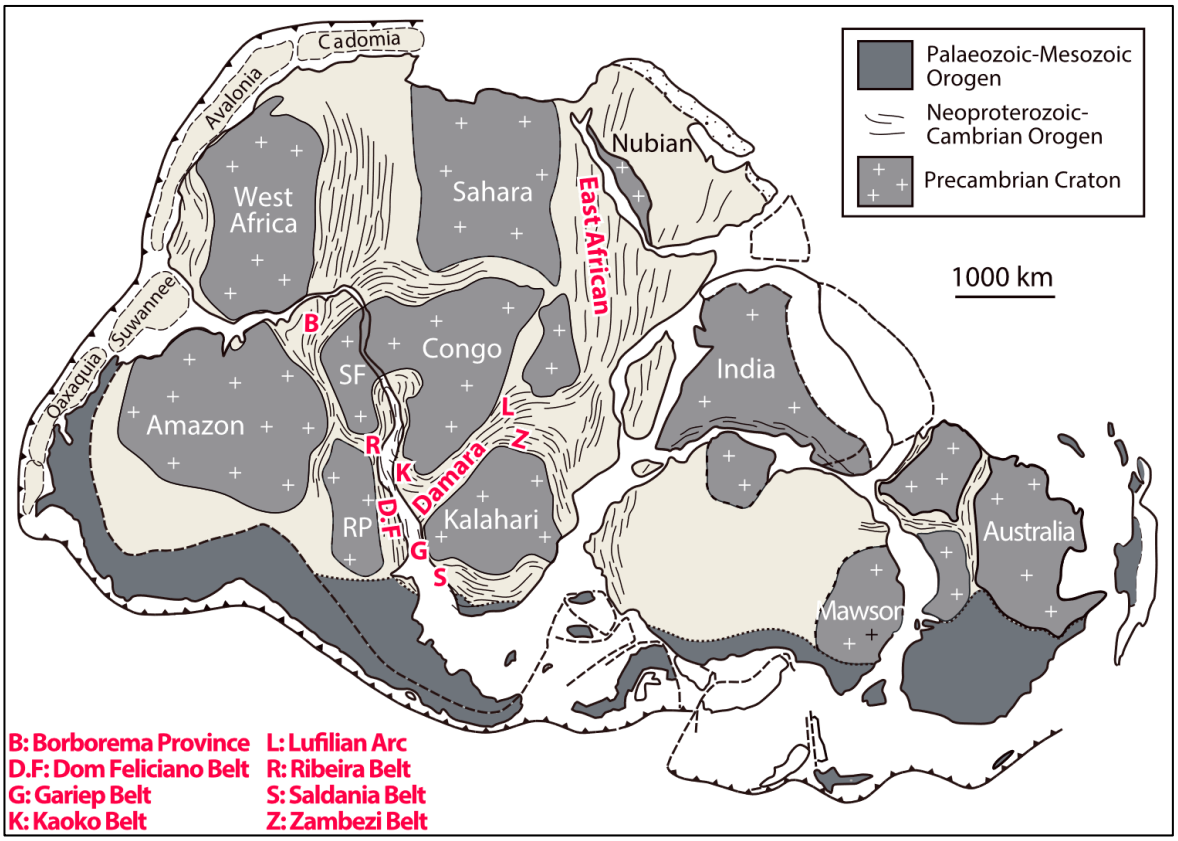

Figure 2 – Map of Gondwana in early Cambrian time, showing the collage of continental cratons assembled along a network of orogenic belts. After Gray et al. (2008) and Lehman et al. (2015).

4) Results & Observations

4.1 Lithostratigraphic architecture of the Damara Belt

The metasedimentary succession of the Damara Belt encompasses:

Northern and Central Zones: A lower rift-related Nosib Group - composed of debrites and cross-bedded arkoses – was deposited in an alluvial fan setting at c. 870-760 Ma. In the Northern Zone, this progressed to slope and proximal submarine fan successions of the lower Otavi Group at c. 760-635 Ma, followed by medium to distal submarine fan deposits of the upper Otavi Group at c. 663-590 Ma (Nascimento et al., 2016, 2017). The Central Zone preserves a similar stratigraphic succession; lower rift-related Nosib Group sediments are overlain by passive margin sequences of the Swakop Group (Henry, 1992; Lehtonen et al., 1996; Miller, 2008). The Swakop Group in the Central Zone has been correlated with the Otavi Group in the Northern Zone (Nascimento et al., 2016).

In addition, the Central Zone is often suggested to preserve c. 1-2 Ga pre-Damaran basement outcrops in the cores of some dome structures, in the form of a heterogeneous assemblage termed the Abbabis Complex (Smith, 1965; Marlow, 1981; Barnes, 1981; Sawyer, 1979; Jacob et al., 1983; Brandt, 1987; Longridge, 2012). However, several exposures of the Abbabis Complex have since been reinterpreted as a migmatite-granite terrain formed from crustal melting and granite intrusion into the Damara Supergroup during the Damara Orogeny; this includes at the Rossing Dome (Oliver and Kinnaird, 1996) and large exposures along the lower Swakop River (Toe et al., 2013; Jones et al., 2026).

Khomas Complex: The Khomas Complex consists almost entirely of imbricated metaturbidites (Kukla and Stanistreet, 1991). These can be correlated with the Kuiseb Formation at the top of the Swakop/Otavi groups. A narrow 500-3,000 metre wide unit of mafic metavolcanic and plutonic rocks with Mid Ocean Ridge Basalt geochemistry is imbricated with the metaturbidites; this can be traced along strike for over 300 km (Figure 3; Meneghini et al., 2017).

Southern Marginal Zone: The Southern Foreland / Southern Marginal Zone separates the Khomas Complex from the bounding Kalahari Craton (Figure 3). It consists of tectonically imbricated metasedimentary units and metabasite lenses (Hartnady, 2014), as well as interleaved thrust sheets of pre-Damaran basement material (Miller, 1983 and references therein, p. 463).

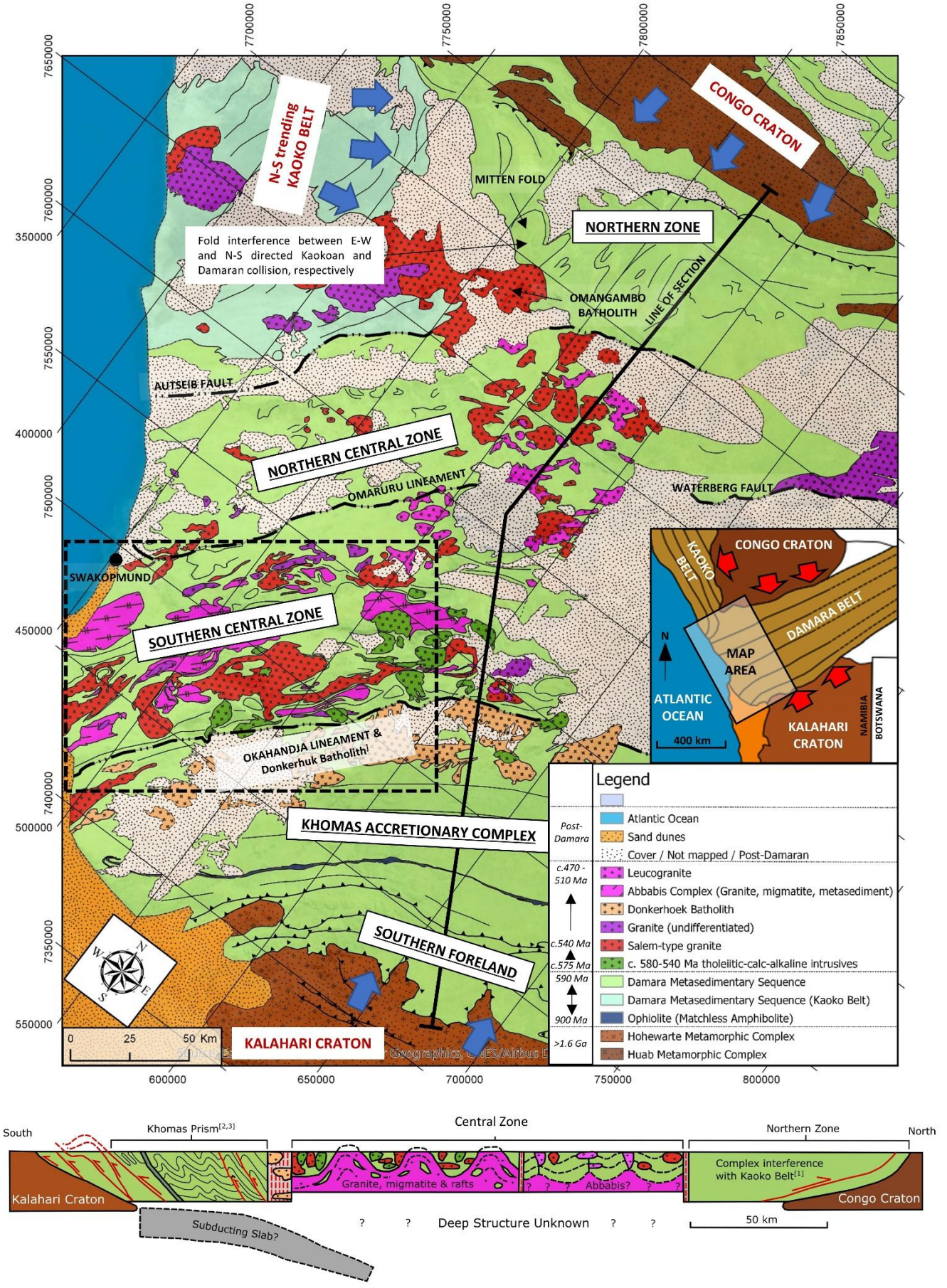

Figure 3 - Regional geological map and interpretative cross-section of the Damara Orogen, modified after Miller and Grote (1988), Geological Survey of Namibia (Sheets 2214, 2216, 2116, 2114, 2014), and Knupp (2019). Dashed black box highlights approximate area of the southern Central Zone mapped in Figure 7.

4.2 Magmatic architecture and 2-stage evolution of igneous activity

Igneous rocks of the Damara Orogen are concentrated mainly in the Central Zone, with the southern Central Zone hosting the largest volume of igneous intrusions. Igneous activity extended into parts of the Northern Zone in the form of the giant Omangambo Batholith. The Khomas Complex and Southern Foreland in contrast experienced very little magmatic activity (Figure 3).

2-stage igneous evolution: Igneous activity evolved progressively, from early tholeiitic to calc-alkaline magmatism at c. 575-540 Ma, followed by later leucogranite magmatism at c. 530-500 Ma. A time lag of ~20-30 Myr separated the cessation of early calc-alkaline to tholeiitic magmatism from the peak of leucogranite magmatism at c. 510 Ma (Figure 4). For data sources see Table 1 in Apppendix I.

Early c. 575-540 Ma tholeiitic to calc-alkaline magmatism: Early mafic magmatism has a dominantly crustal signature as indicated by sub-chondritic εHf_t values (-3.8 to -34.4) (Milani et al., 2015). However, processes including mantle melting, fractional crystallisation, accumulation, and local assimilation have all been invoked to explain diverse compositions within this igneous suite. The extent to which early tholeiitic and calc-alkaline magmatism reflects classical subduction initiation, versus an alternate model of flat subduction and/or ensialic reworking of old lithospheric crust, is disputed (Milani et al., 2015; Jung et al., 2020a; Clemens and Kisters, 2021; Clemens, 2022; Jung and Romer, 2024; Hars et al., 2025).

Later c. 530-510 Ma leucogranite magmatism has an overwhelmingly crustal signature. Most leucogranites are peraluminous S-type granites derived from partial melting of metasedimentary source rocks (Jung et al., 1995; Jung et al., 2001; Ward et al., 2008; Paul et al., 2013; Ashworth et al., 2020). A smaller subset of leucogranite formed from partial melting of meta-igneous crust and mixed metasedimentary + igneous crustal sources (Jung et al., 2009; Ashworth et al., 2020).

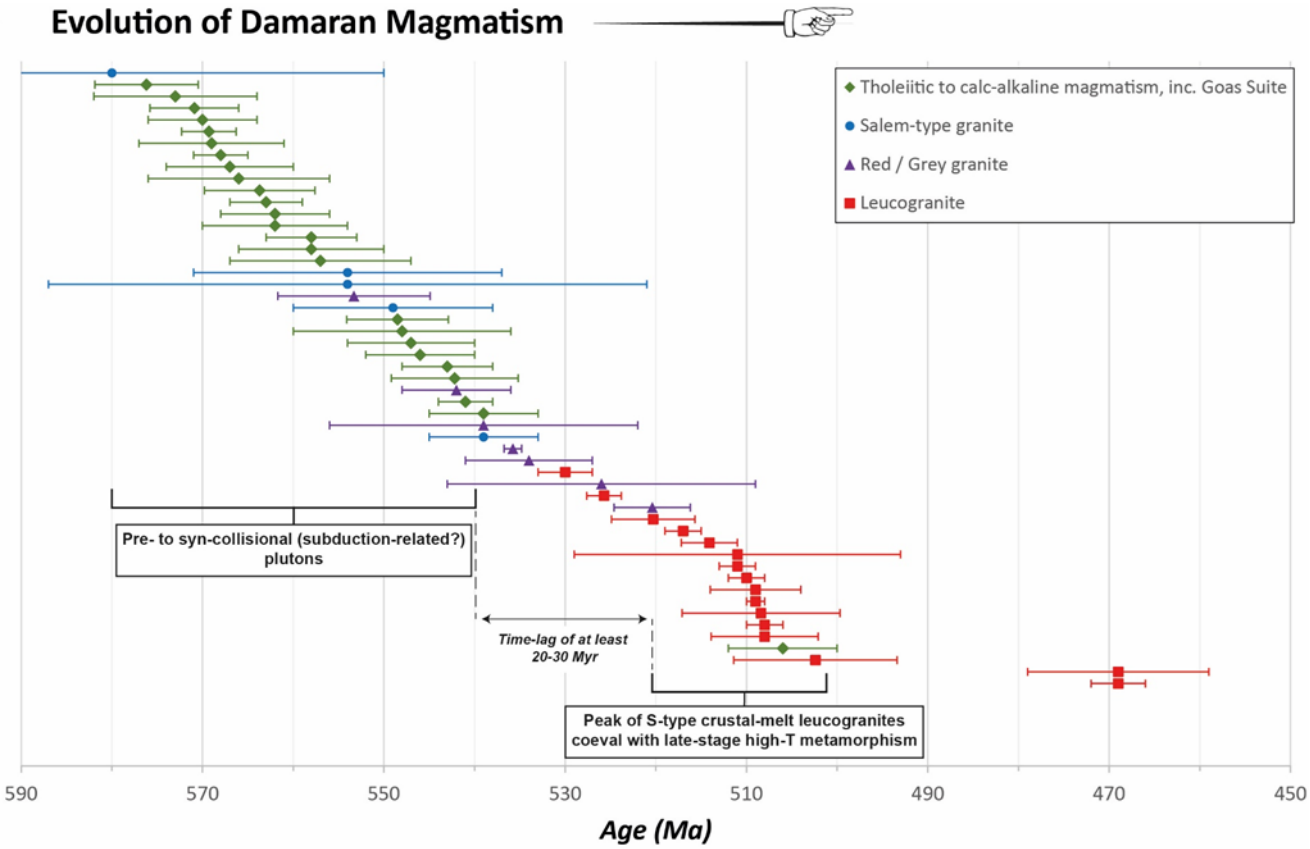

Figure 4 – Compilation of igneous rock ages from the Central Zone of the Damara Orogen. For data sources see Table 1 in Appendix I.

4.2 Metamorphic architecture of the Damara Belt

An interpretive metamorphic isograd map of the Damara Orogen is presented in Figure 5, based on the work and synthesis of Goscombe et al. (2017b). The metamorphic architecture encompasses:

High-temperature Central Zone: The Central Zone is characterised by high-temperature Buchan series metamorphic fields (Figure 5). Medium-pressure (~4-5 kbar) granulites show concentric zonation from highest grade garnet-cordierite-k-feldspar-plagioclase-melt in the central west, decreasing outward to the north, south and east across melt-out, plagioclase-out, sillimanite-plagioclase-in, and k-feldspar-out isograds (Figure 5; Goscombe et al., 2017b). Peak metamorphic temperatures exceeded 800^{O}C on a regional basis throughout the southwestern Central Zone; the heating path to peak granulite-facies conditions occurred isobarically at a consistent pressure of 4-5 kbar (Longridge et al., 2017; Jung et al., 2019; MacRoberts et al., 2025).

Low-temperature high-pressure bounding wedges: The bounding Northern and Southern Zones of the orogen are defined by higher-pressure lower-temperature Barrovian metamorphic fields (Figure 5). Metamorphic isograds, thrusts and main foliation are sub-parallel and inclined shallowly towards the north in the Southern Zone. In the Northern Zone, a high-P/low-T metamorphic gradient is similarly inverted; metamorphic zonation shows overall southward increase in grade across the muscovite-in, biotite-in, garnet-in, staurolite-in, and kyanite-in isograds (Figure 5; Goscombe et al., 2017b). Peak pressures reached ~10-11 kbar in the Northern and Southern zones (Goscombe et al., 2017b), higher than the 4-5 kbar recorded in the southern Central Zone (Longridge et al., 2017; Jung et al., 2019; MacRoberts et al., 2025).

Okahandja Lineament Zone & Donkerhuk Batholith: The Okahandja Lineament Zone separates the Central Zone from the southern Zone and has a complex metamorphic pattern, characterised by an elongate along-strike high-grade thermal anomaly. Metamorphic zonation crosses the sillimanite-in, k-feldspar-in, muscovite-out and sillimanite-out isograds, reaching garnet-cordierite-biotite-k-feldspar-plagioclase-melt and cordierite-spinel parageneses (Figure 5; Goscombe et al., 2017b and references therein). The Okahandja Lineament Zone is spatially associated with the giant S-type Donkerhoek Batholith - for detailed studies see Clemens et al. (2017a, 2017b) and Jung and Hauff (2021).

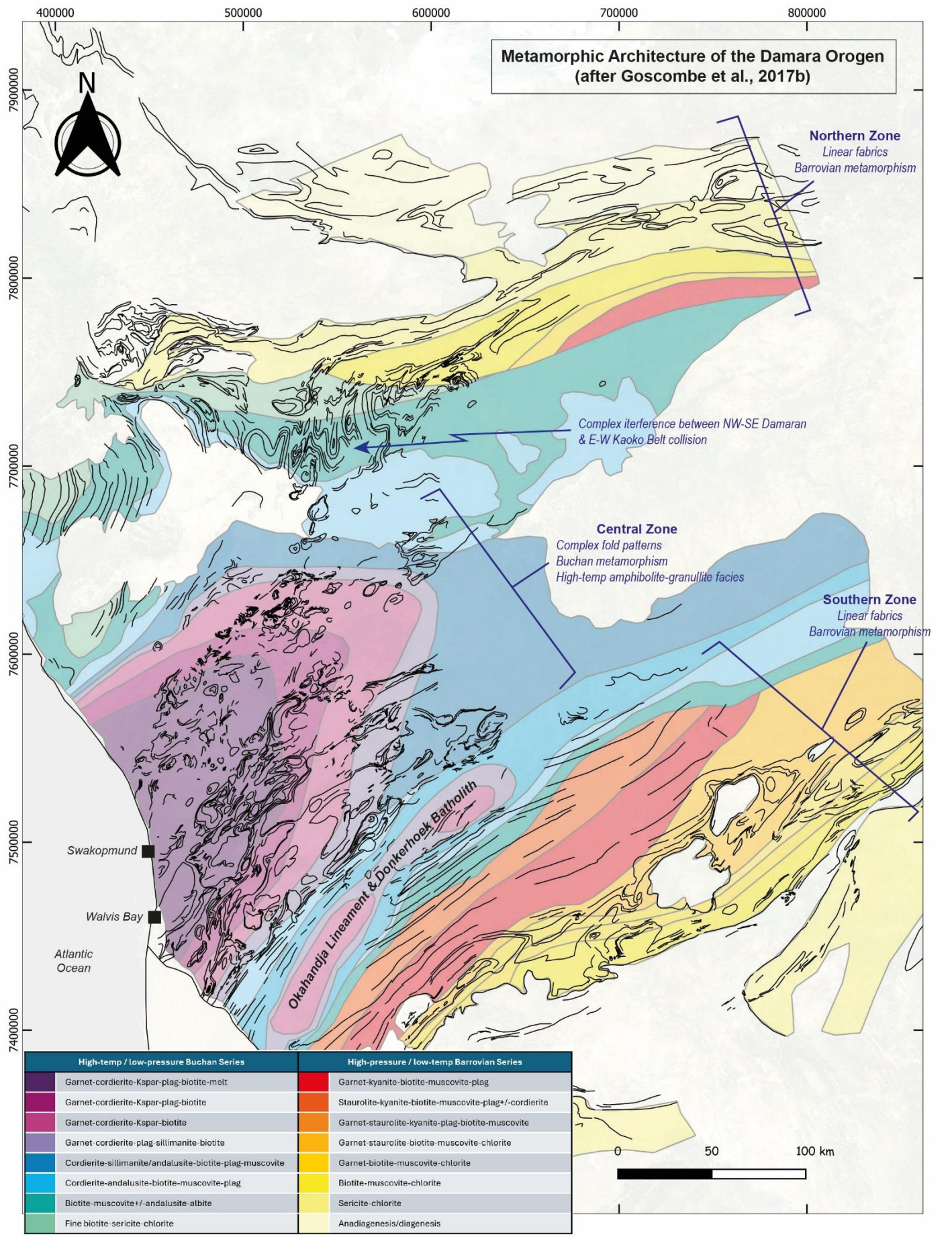

Figure 5 - Interpretive metamorphic isograd map of the Damara Orogen, simplified slightly from the work of Goscombe et al. (2017b). Coordinate system = UTM Zone 33 S.

4.3 Macro structural fabric patterns in the Damara Belt

The Damara Belt trends inland across Namibia, stretching from the Atlantic coastline towards the NE. The Huab Metamorphic Complex and the Rehoboth Inlier bound the Damara Belt to the north and south, respectively. The NNW-SSE trending Kaoko Belt outcrops in the northwest of the study area. Structural fabric patterns show pronounced changes in structural style across different zones of the Damara Belt (Figure 6):

Northern Platform: The Northern Platform outcrops north of the Huab Metamorphic Complex and trends inland towards the ENE. The Northern Platform is characterised by relatively simple linear ENE-trending fabrics, including some tight ENE-trending fold axes (Figure 6).

Northern Zone: The Northern Zone displays a more complex structural pattern (Figure 6). Simpler NE-SW trending fabrics in the far northeast become folded around a Ramsay Type-2 fold interference structure further to the west. The Type-2 fold interference structure is centred on the Mitten Fold (Figure 6), effectively marking the transition between NE-SW trending Damaran fabrics and NNW-SSE trending Kaoko Belt fabrics to the west. This Type-2 fold interference structure forms a largely consistent pattern across the exposed portion of the Northern Zone.

Central Zone: The Central Zone displays the most complex fabric pattern in the Damara Belt (Figure 6). Structural fabrics have a predominant NE-SW trend; however, complex domes, basins, and fold interference patterns dominate.

Khomas Complex: The Khomas Complex displays highly linear NE-SW trending fabrics which contrast sharply with the complex folds of the Central Zone to the northwest. Isoclinal NE-SW trending folds are locally observed amongst the linear fabrics (Figure 6).

Southern Marginal Zone: The Southern Marginal Zone displays predominantly NE-SW trending structural fabrics, punctuated by tectonic window structures exposing underlying basement rocks of the bounding Kalahari craton (Figure 6).

Naukluft Nappe Complex: Exposed in the far south of the study area, this again shows a predominantly NE-SW trend consistent with the regional trend of the Damara Belt (Figure 6).

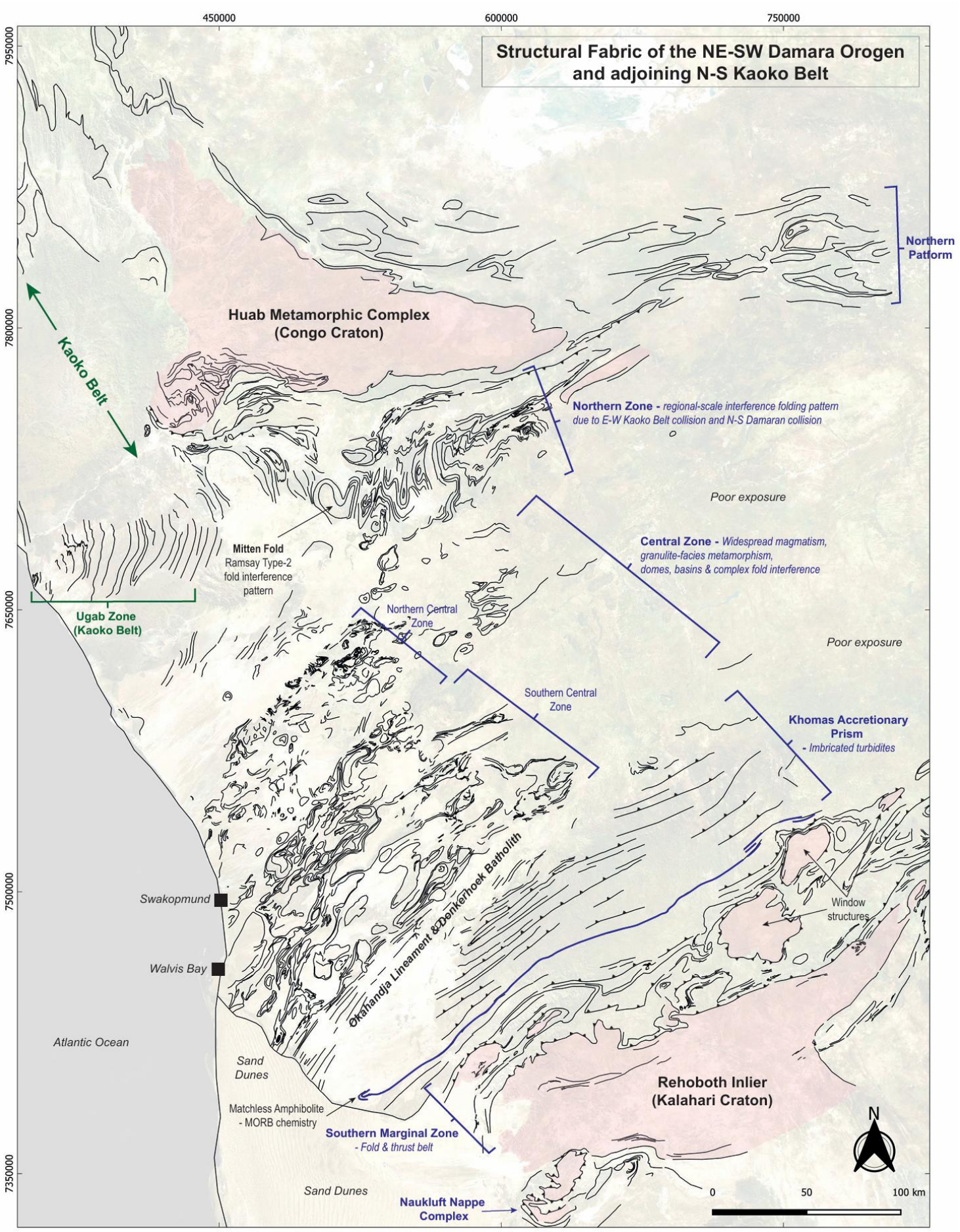

Figure 6 - Structural fabric map of the Damara Belt in western Namibia. Coordinate system = UTM Zone 33 S.

4.4 Complex structural fabric patterns in the Central Zone

The complexity of fold and fabric patterns in the Central Zone is anomalous against the more linear NE-SW trending fabrics of the Northern and Southern Zones (Figure 6). A detailed structural fabric map of the southern Central Zone is presented in Figure 7. Key observations include:

4.4.1 Diversity of fold patterns

A wide variety of fold styles are observed across the southern Central Zone (Figure 7). Folds are heterogeneous, disharmonic, and non-cylindrical. Fold axes are typically highly curvilinear. Fold structures span a range of scales, from <1 km to nearly 100 km in along-strike extent. Larger elongate fold structures such as the Abbabis Dome host smaller second-order folds within them. Fold aspect ratios are highly variable; some have aspect ratios as low as 2:1, such as the Rossing Dome, Ida Dome, and Rossing Mountain Dome, while others such as the Husabberg Anticlinorium, Abbabis Dome and Rooikuiseb Anticlinorium have aspect ratios as high as 9:1. Fold interference structures are common but highly variable. Examples corresponding to all three interference types of Ramsay (1962) are observed; classical Type-1 dome-and-basin structures are observed at the Rossing Dome, Type-2 boomerang or arrowhead shapes are observed at the Rossing Mountain Dome, and Type-3 hook-shaped folds are also locally observed. However, many fold structures display complex morphologies that cannot be readily classified within the Ramsay Type 1–3 scheme; examples include the Tumas Dome and the Ruby Substation Dome (Figure 7).

Fold geometries and styles vary across the southern Central Zone and are not restricted to discrete structural domains. Examples of individual fold structures are shown in the panels of Figure 8:

Figure 8A / Rossing Mountain Dome: Most closely matches a Ramsay (1962) Type-2 fold interference structure, with a boomerang / arrowhead pattern.

Figure 8B / Interlocking folds immediately SW of Rossing Mountain: Occurring immediately SW of the Rossing Mountain Dome, the interlocking nature of domes and basins here more closely resembles a Ramsay Type-1 interference pattern.

Figure 8C / H-shaped fold NW of Rooikuiseb Anticlinorium: A major H-shaped fold structure in the 10s km scale which does not cleanly conform to any Ramsay interference pattern.

Figure 8D / Namibfontein-Vergenoeg double dome: Top-half of the panel shows the Namibfontein-Vergenoeg double-dome structure, with two smaller domes visible in the bottom half of the panel. The overall geometry does not correspond clearly to a Ramsay interference fold type.

Figure 8E / Tumas Dome: Displays a complex morphology comprising two subdomains and a kilometre-scale hook-like structure near their boundary; the overall geometry cannot be readily classified within the Ramsay interference fold scheme.

Figure 8F / Abbabis Dome: A major elongate structure extending for ~100 km along strike, containing smaller second-order fold structures.

Figure 8G / Husabberg Anticlinorium: Another large, elongate dome extending for >70 km along strike.

Figure 8H / Unnamed dome east of Husab Mountain: A comparatively simple NE–SW trending dome demarcated by a marble rim and developed within a surrounding Salem-type granite batholith.

Figure 8I / Open fold zone south of the Tumas Dome: A zone in which the dominant NNE–SSW structural grain is disrupted by NW–SE trending open folds in marble units, producing a complex fold pattern. Such heterogeneity is not uncommon in marble units within the southern Central Zone.

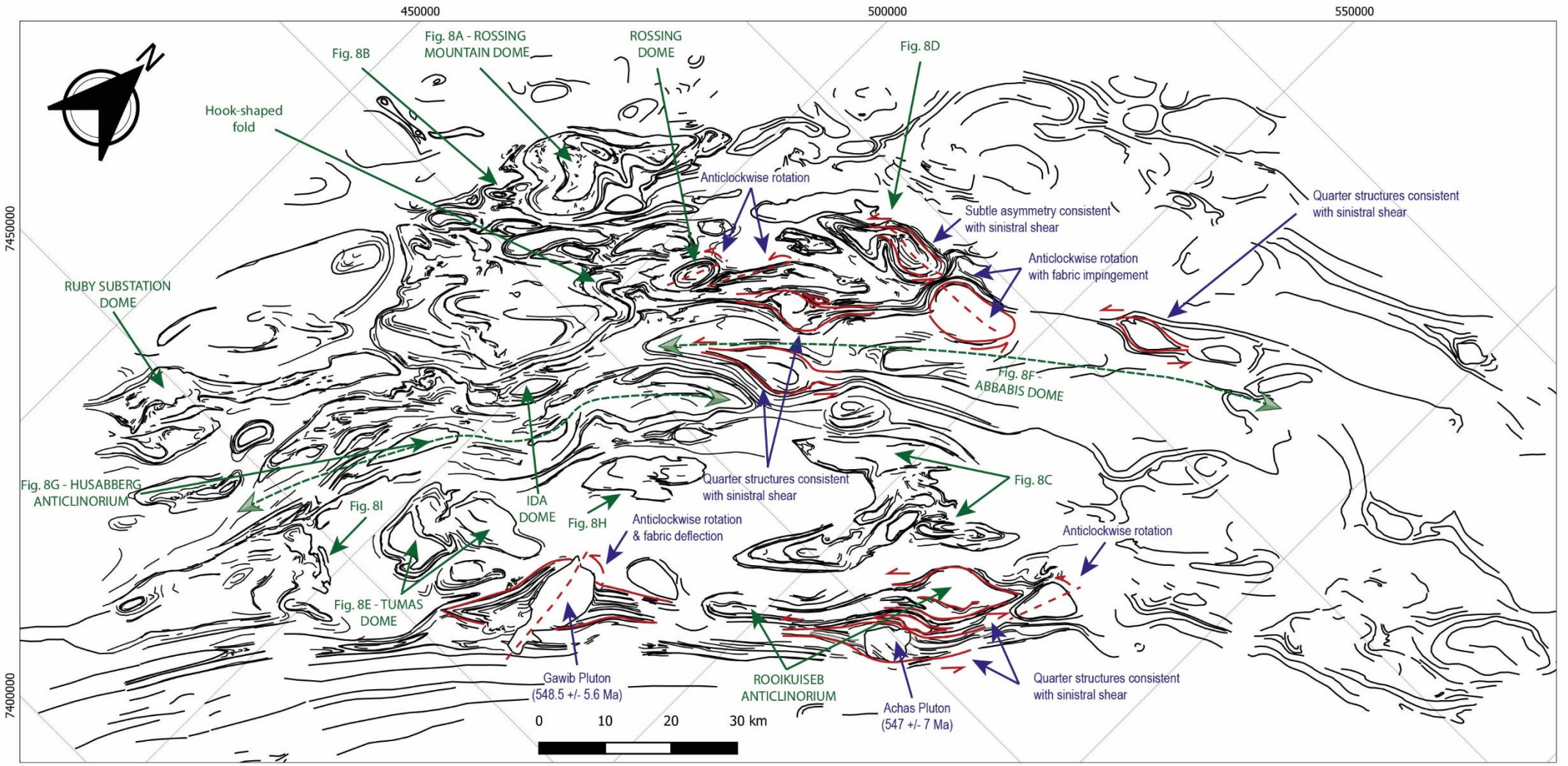

Figure 7 - Detailed structural fabric map of the southern Central Zone created from an interpretation of satellite and aeromagnetic data. Note the complexity and variety in morphology of domes and fold interference patterns observed throughout the southern Central Zone. Labelled domes are discussed in the main body text. Coordinate system = UTM Zone 33 S.

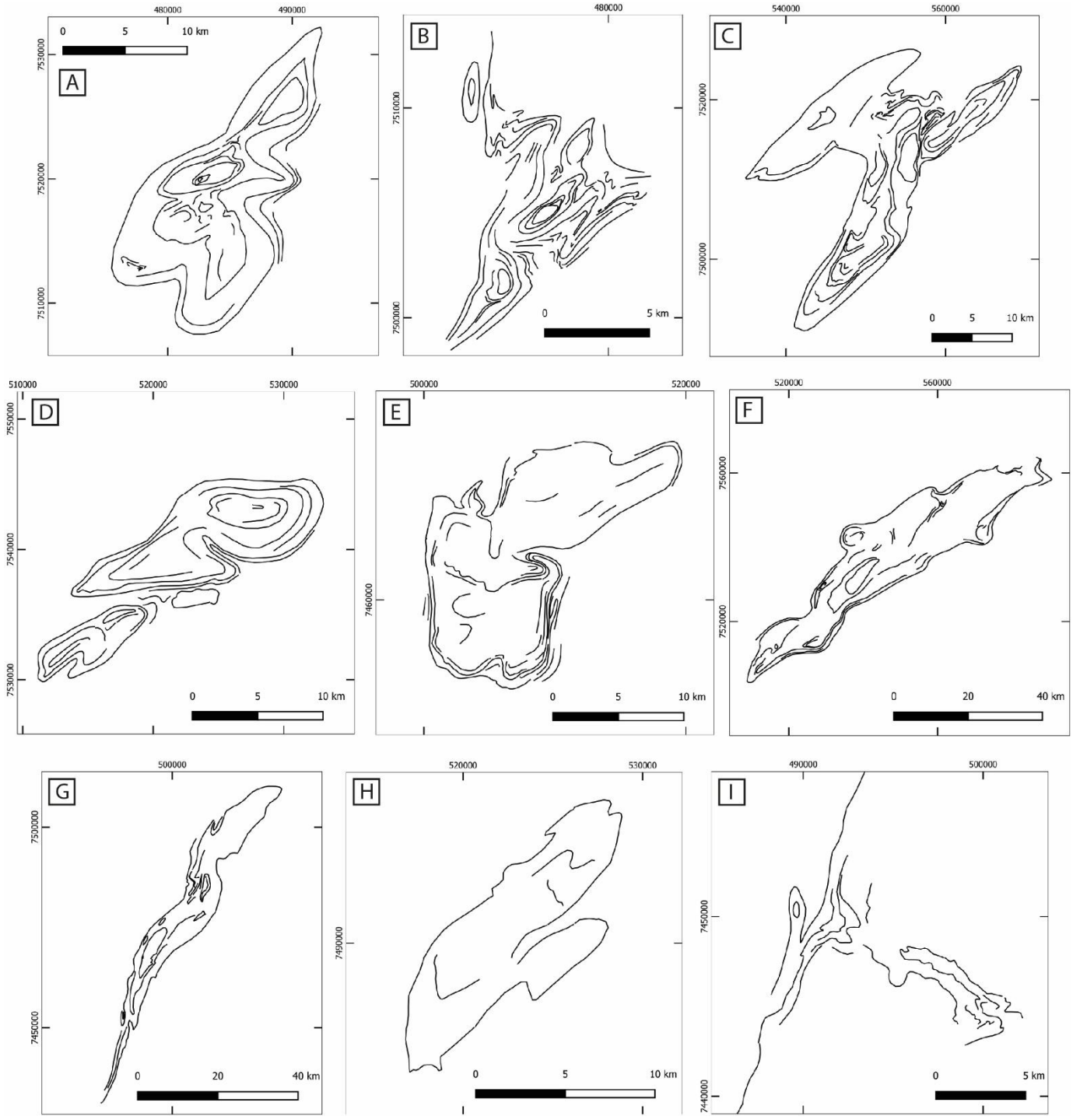

Figure 8 – Panel image showing selected examples of fold patterns in the southern Central Zone, mapped from satellite and aeromagnetic data. A) Rossing Mountain fold. B) Interlocking dome-and-basin structures immediately south of Rossing Mountain. C) H-shaped fold structure immediately NW of the Rooikuiseb Antlclinorium. D) Namibfontein-Vergenoeg double dome structure. E) Tumas Dome. F) Abbabis Dome. G) Husabberg Anticlinorium. H) Unnamed dome east of Husab Mountain. I) Open fold zone south of the Tumas Dome. Coordinate system = UTM Zone 33 S.

1

2

3

4

4.4.2 Kinematic indicators

Asymmetric sense-of-shear indicators are variably developed throughout the southern Central Zone; they imply a consistent orogen-parallel sinistral sense of shear (Figures 7 and 9). Kinematic indicators include quarter structures (Figure 9A & 9B) and anticlockwise rotation of both km-scale dome structures and granitic plutons (Figure 9A to 9D). Subtle S-C structures are also visible throughout the southern Central Zone in the 1st Vertical Derivative of aeromagnetic data (Figure 9E). The Achas Pluton and Gawib Pluton shown in Figure 9B and 9C have been dated at 547+/-7 Ma and 548.5 +/- 5.6 Ma, respectively (Osterhus et al., 2014; Simon et al., 2017).

It is noted that kinematic indicators consistent with sinistral shear appear to be subordinate to the complex heterogeneous fold structures described above, in terms of their overall prominence in the regional architecture of the southern Central Zone (Figure 7).

4.4.3 Contrasting rheological response to deformation

Satellite imagery preserves evidence for different rheological responses to deformation across different rock units in the southern Central Zone. Major km-scale dome structures are typically cored by massive granites, migmatites, and/or quartzite units which lack strong layering or foliations. These frequently show evidence for rigid behaviour and anticlockwise rotation amongst the surrounding gneisses and schists (Figure 9A-D). Meanwhile, the intervening gneiss and schist units which mantle the domes, and have a strong anisotropy defined by foliation, are commonly pinched, wrapped and squeezed between the larger dome structures (e.g. Figure 9D).

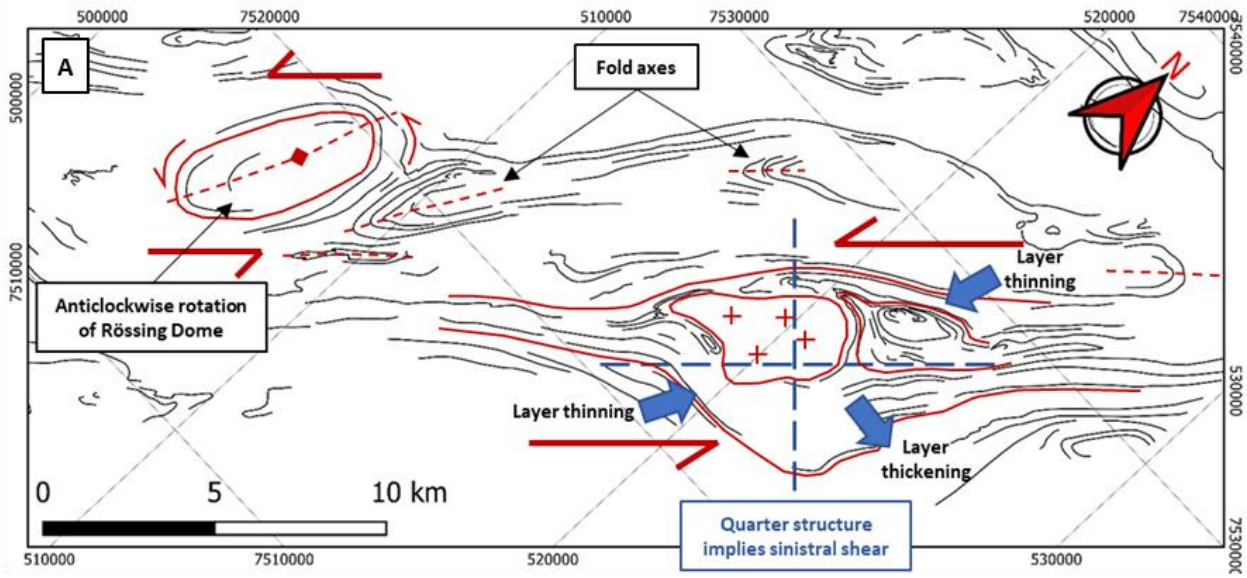
A
Fold axes
Anticlockwise rotation of Rössing Dome
Layer thinning
Layer thinning
Layer thickening
Quarter structure implies sinistral shear
0 5 10 km
500000
7520000
510000
7530000
520000
7540000
7510000
530000

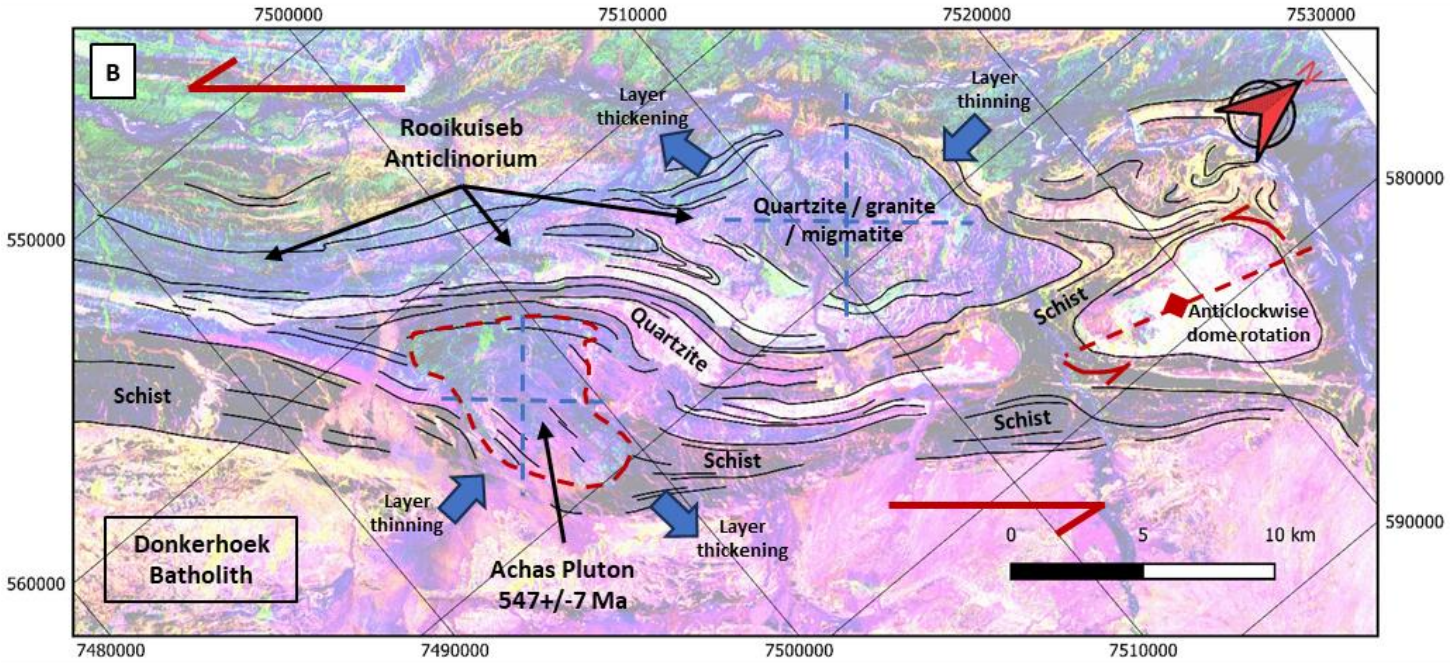
B
Rooikuiseb Anticlinorium
Layer thickening
Layer thinning
Quartzite / granite / migmatite
Quartzite
Schist
Schist
Schist
Schist
Anticlockwise dome rotation
Layer thinning
Layer thickening
Donkerhoek Batholith
Achas Pluton 547+/-7 Ma
0 5 10 km
7500000
7510000
7520000
7530000
550000
560000
580000
590000
7480000
7490000

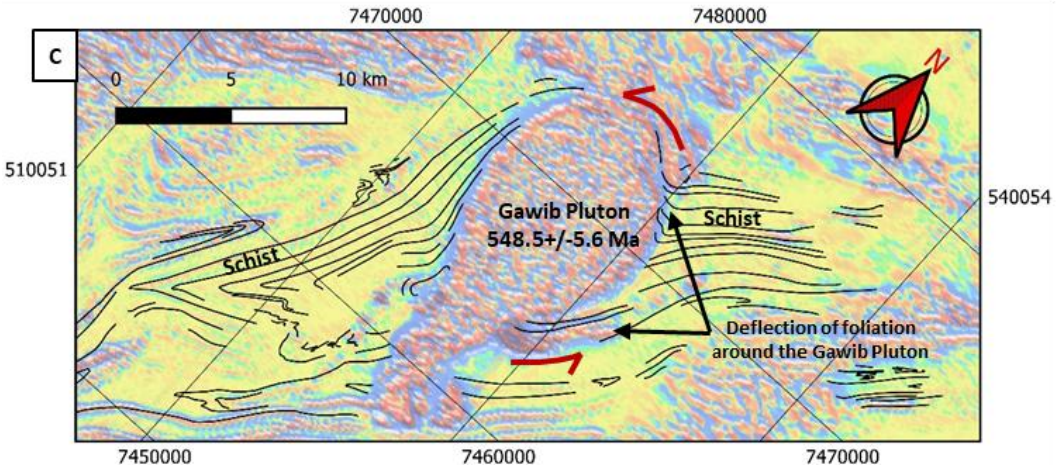
C
0 5 10 km
Gawib Pluton 548.5+/-5.6 Ma
Schist
Schist
Deflection of foliation around the Gawib Pluton
7470000
7480000
510051
540054
7450000
7460000

40

41

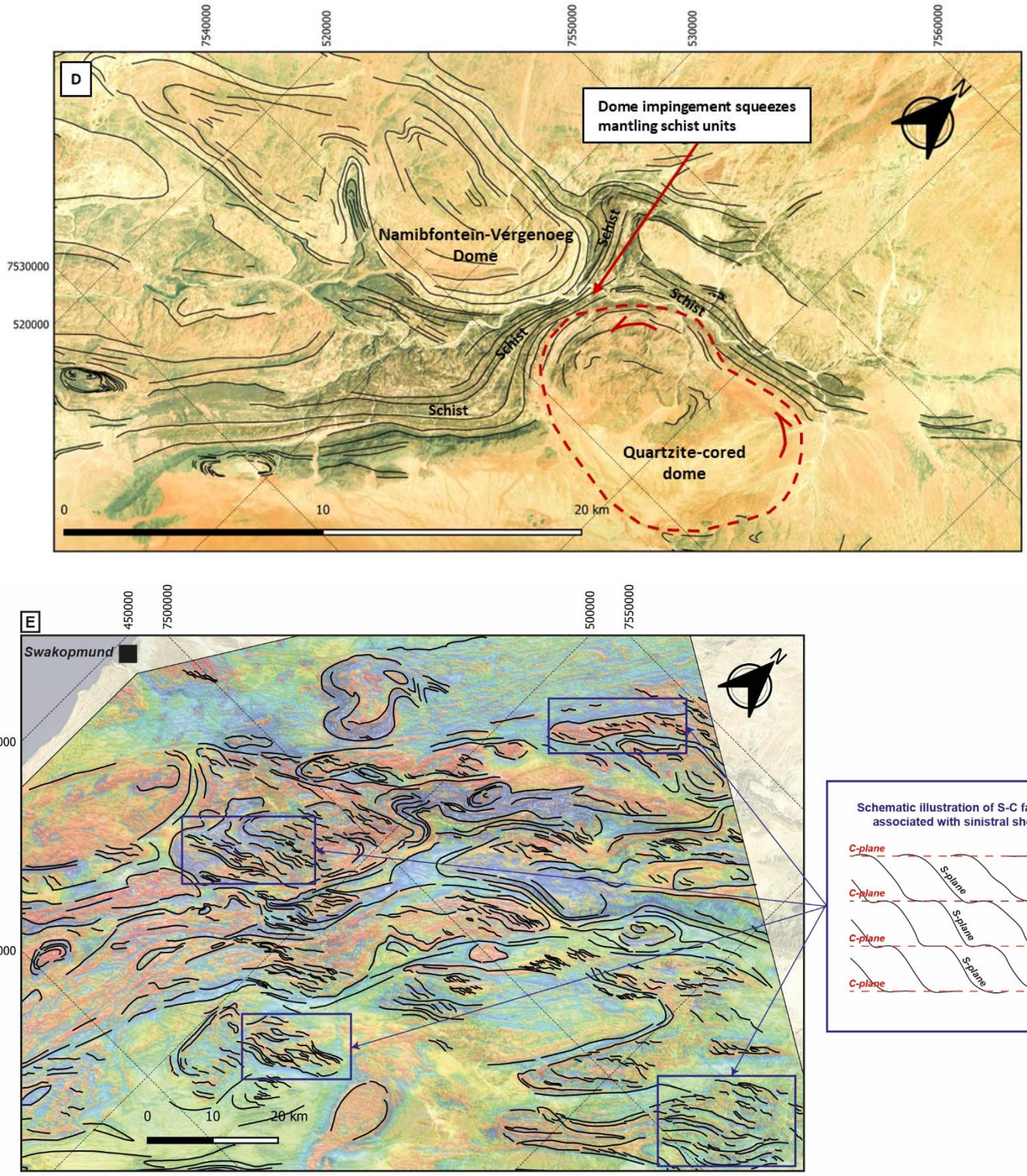

Figure 9 – Asymmetric sense-of-shear indicators observed in regional datasets throughout the southern Central Zone. A) Fabric map showing quarter structures and anticlockwise dome rotation in the vicinity of the Rossing Dome. B) Quarter structures and anticlockwise dome rotation at the Rooikuiseb Antliclinorium and Achas Pluton, shown on ASTER data – Achas Pluton dated at 547 Ma by Simon et al., 2017. C) Anticlockwise rotation of the Gawib Pluton associated with deflection of mantling schist units – pluton dated at 548.5 Ma by Osterhus et al., 2014. D) Bing satellite image showing anticlockwise rotation of a quartzite dome and impingement against the neighbouring Namibfontein-Vergenoeg Dome E) Subtle S-C fabrics visible throughout the southern Central Zone in the 1st vertical derivative of aeromagnetic data. Coordinate system = UTM Zone 33 S.

42

43

4.4.4 Distributed deformation in migmatites

The Ida Dome is an example of a km-scale dome cored by Damaran-aged leucogranites and migmatites in the southern Central Zone (Toe et al., 2013; Jones et al., 2026). Field observations reveal that migmatites contain asymmetric fabrics consistent with widespread ductile shearing over large outcrop areas (Figure 10). There is little evidence for strain localisation into distinct faults or shear zones. Top-to-the-SE reverse shear on this NW-dipping limb (Figure 10) is mimicked by top-to-the-NW reverse shear on SE-dipping dome limbs, consistent with overall bulk coaxial shortening in this area. Distributed deformation and widespread syn-magmatic constrictional strains are documented throughout several dome structures within and immediately south of the lower Swakop River (Jones, 2026).

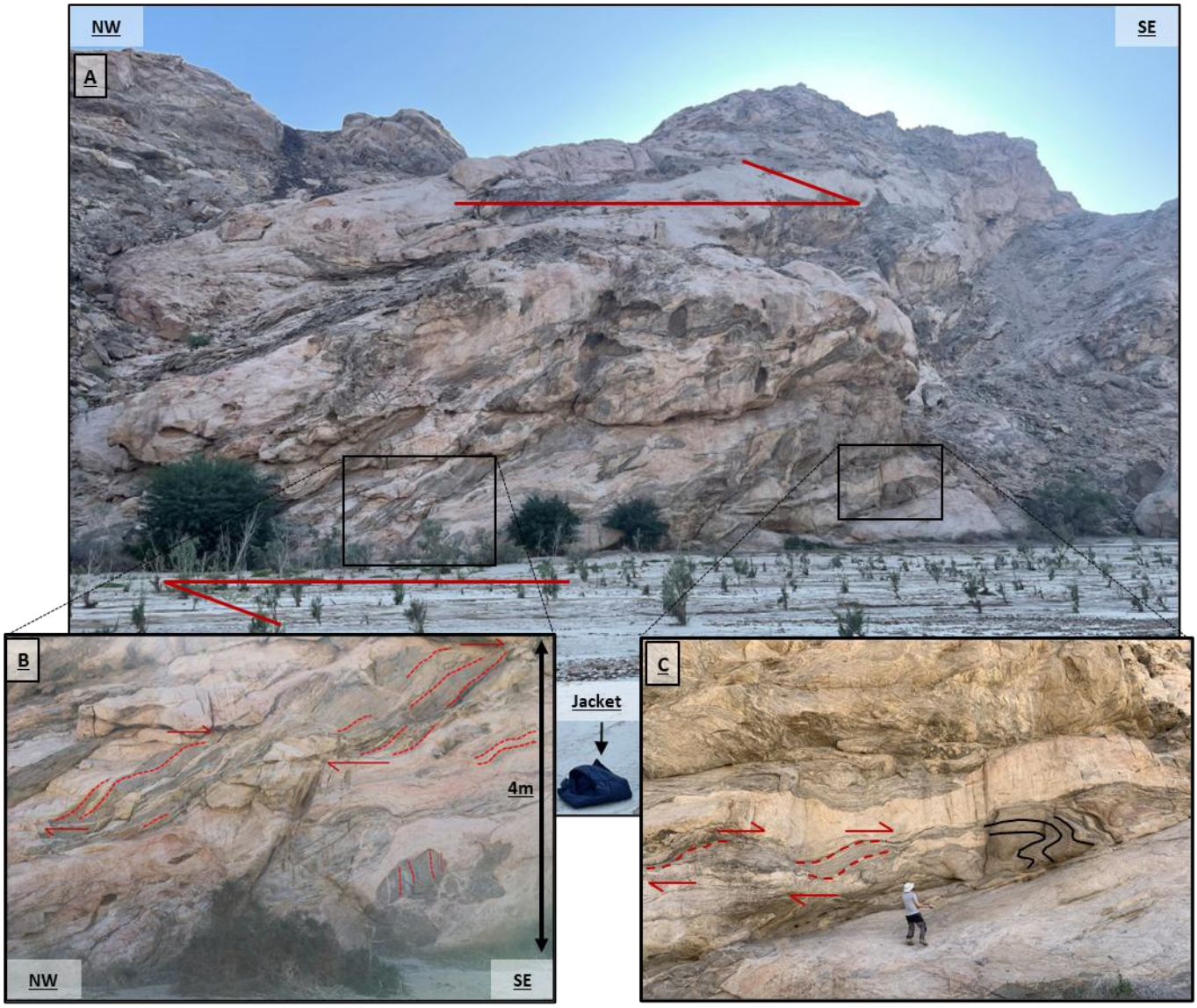

Figure 10 – Field example of distributed deformation in leucogranites and migmatites in the core of the Ida Dome, southern Central Zone. Asymmetric fabrics on this NW-dipping dome limb record apparent top-to-the-SE reverse kinematics.

5) Interpretation & Discussion

5.1 Does the Damara Belt fit a hot-orogen model?

The first-order architecture of the Damara Belt closely matches the conceptual "hot-orogen" model of Jamieson and Beaumont (2013; Figure 1 and Figure 11). Key criteria include:

1. ***A paired metamorphic architecture:*** The HTLP Central Zone is bookended by back-to-back LTHP inverted Barrovian metamorphic sequences in the Northern and Southern zones (Figure 6 and Figure 11).
2. ***A paired structural architecture:*** Complex fold and fabric patterns in the HTLP Central Zone are bookended by oppositely dipping critical wedges in the LTHP Northern and Southern zones (Figure 6, 7 and 11).

   The HTLP Central Zone records distributed deformation in migmatitic rocks (Figure 10), as well as NW-SE shortening and widespread orogen-parallel constrictional strains developed coevally with leucogranite magmatism (Poli and Oliver, 2001; Kruger and Kisters, 2016; Jones, 2026). Complex local overprinting relationships are widely reported at individual dome structures (Jacob et al., 1983; Ormond et al., 2024).

   In contrast, the bounding LTHP Northern and Southern Zones are defined by simpler melt-absent non-coaxial folding and thrusting towards the bounding cratonic margins. This is manifested in E-W to NE-SW striking fold trains, axial planar cleavages, down-dip lineations, and consistent foreland-vergent kinematic indicators (Miller, 1983 *and references therein*; Kukla and Stanistreet, 1991; Rowe et al., 2012; Hartnady, 2014; Meneghini et al., 2014, 2017; Kitt et al., 2016, 2018; Lehmann et al., 2016; Passchier et al., 2016).
3. ***The magmatic architecture correlates with the structural-metamorphic architecture***: Large volumes of igneous rocks in the Central Zone (Figure 3) are spatially associated with HTLP Buchan-series metamorphism (Figure 5) and complex fold and fabric patterns (Figures 6-10). In contrast, limited magmatic activity in the bounding Northern and Southern zones (Figure 3) is associated with LTHP Barrovian-series metamorphism (Figure 4) and simpler linear fabric patterns (Figure 6).
4. ***A 2-stage tectono-magmatic evolution encompassing early tholeiitic to calc-alkaline magmas, followed by crustal-melt leucogranites ~20-30 Myr later (Figure 4)***: This is a characteristic signature of many hot-orogens, where early arc- or syn-collisional magmatism is followed by a second stage of crustal-melt leucogranites ~20-30 Myr later (Jamieson and Beaumont, 2013).

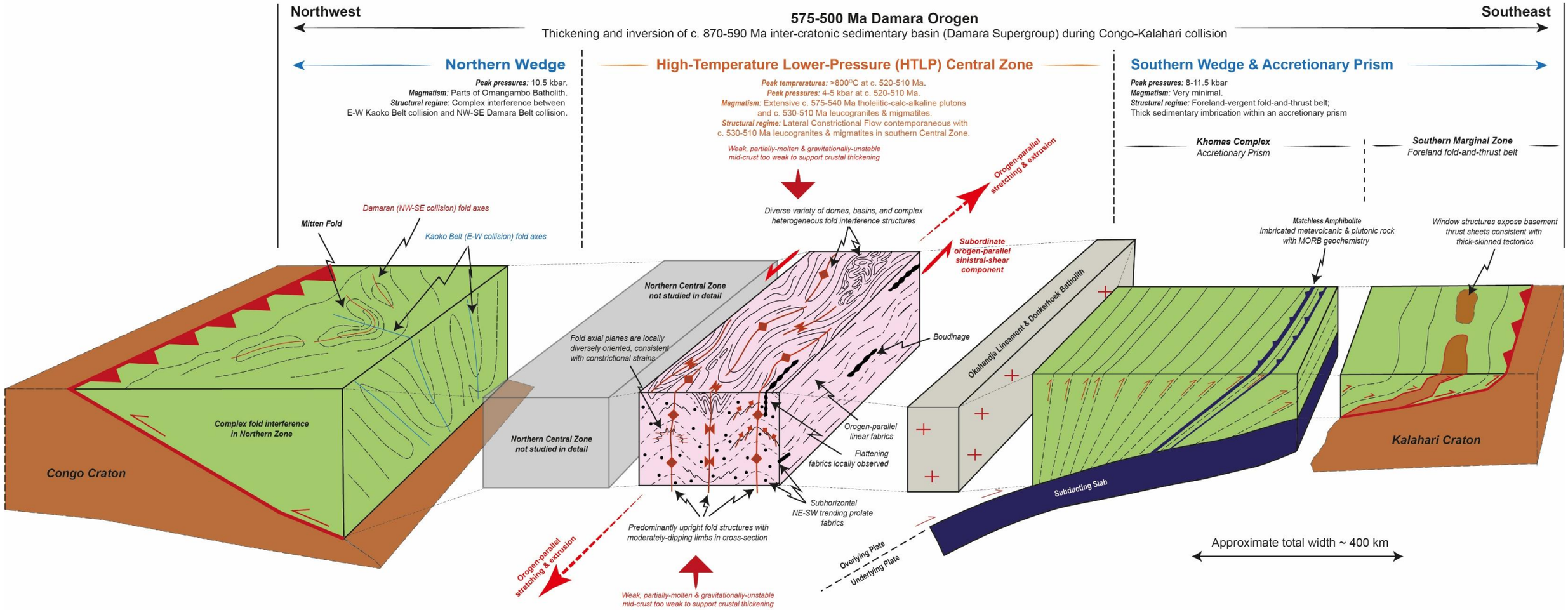

Figure 11 – Interpretive 3D block model showing variations in structural style across different zones of the Damara Orogen. The Northern Zone is complicated by interference between Kaoko and Damara Belt collision. The interior Central Zone is dominated by orogen-parallel linear fabrics and complex heterogeneous fold interference structures. The bounding Southern Zone displays accretionary prism and fold-thrust belt geometry. The overall architecture approximately comprises of oppositely dipping wedges bounding a HTLP Central Zone.

5.2 Heat sources driving high-temperature low-pressure (HTLP) metamorphism and widespread leucogranite magmatism in the Central Zone

Peak metamorphic temperatures exceeding 800^{O}C led to widespread partial melting and leucogranite magmatism in the Central Zone at c. 530-510 Ma (Figure 4). This lagged earlier tholeiitic to calc-alkaline magmatism by 20-30 Myr (Figure 4; Longridge et al., 2017; Jung et al., 2019; MacRoberts et al., 2025).

Radioactive heat production: The time lag of tens of millions of years between early syn-collisional magmatism and peak high-temperature granulite-facies metamorphism is characteristic of long-term heat production from radioactive decay (Th, U, K). Rocks have low thermal diffusivity, meaning crustal thickening effectively insulates the crust and limits heat loss; over long time periods, the energy produced from radioactive decay can raise mid-crustal temperatures by several hundred degrees Celsius. Radioactive heat production is regarded as a critical component in the attainment of regional high-temperature metamorphic conditions in orogenic belts (Clark et al., 2011; Jamieson and Beaumont, 2013; Kelsey and Hand, 2015; Jiao et al., 2023). The contribution of radiogenic heat production to HTLP metamorphism in the Central Zone of the Damara Orogen has been postulated previously (Hartmann et al., 1983; Haack et al., 1983; Jung and Mezger, 2001; Ostendorf et al., 2014; Jung et al., 2026). Radioactive heating is also compatible with the isobaric heating path to peak HTLP metamorphism in the Central Zone (Longridge et al., 2017; Jung et al., 2019; MacRoberts et al., 2025).

Mantle heat: The addition of heat from the mantle is another potential contributor to HTLP metamorphism in the Central Zone, via processes such as slab detachment, asthenospheric upwelling and lithospheric thinning (see discussion in Meneghini et al., 2014; Longridge et al., 2017, 2018). However, peak high-temperature granulite-facies metamorphism at c. 520-510 Ma was associated only with crustal melt leucogranites (Figure 4); the absence of mantle signatures in igneous rocks of this age means that heat addition from the mantle was possible but unproven.

Other heat sources: Additional heat sources include potential latent heat from earlier c. 575-540 Ma tholeiitic and calc-alkaline magmatism – even if these may have cooled significantly by the time of peak HTLP conditions at c. 520 Ma, they could still have further concentrated heat producing elements (Th, U, K) in this portion of the crust, contributing to enhanced radiogenic heat production. Heat may also arise from shear heating along major faults or shear zones (Nabelek et al., 2010), although this is likely to be self-limiting by reductions in shear strength if either partial melt is present or deformation mechanisms switch to diffusion creep at higher temperatures (Clark et al., 2011).

5.3 Deformation style and structural evolution of the HTLP Central Zone

5.3.1 Limitations of traditional structural-tectonic models

The HTLP southern Central Zone of the Damara Orogen is associated with extraordinary structural complexity (Figure 7). Existing tectonic models cannot adequately account for all available data when extrapolated throughout the region:

- *Diapiric upwelling* of domes (Barnes and Downing, 1979; Barnes, 1981; Kroner, 1984) is contradicted by the uniform NE-SW trend of lineations (Poli and Oliver, 2001; Kruger and Kisters, 2016; Jones, 2026), which do not plunge radially outwards from dome cores in the manner predicted by diapiric models (Eskola, 1949). A component of diapirism remains possible, but the consistent trend of orogen-parallel lineations combined with the overall elongate NE-SW trend of dome structures (Figure 7) strongly suggests that plate tectonic forces dominated over diapiric forces.
- *Polyphase deformation* is invoked at individual domes (Jacob et al., 1983; Ormond et al., 2024), but a consistent set of overprinting relations is not observed at the regional scale (Figures 7 and 8). The reported sequence of polyphase deformation also differs between individual domes (e.g. compare Jacob et al., 1983 to Ormond et al., 2024). Together, this suggests that localised overprinting at individual domes probably reflects the effects of progressive strain accumulation in a complex and heterogeneously deforming region, rather than a true polyphase tectonic history which can be attributed to regionally-consistent far-field changes in the boundary conditions during Congo-Kalahari-Rio de la Plata craton collision (see Fossen et al., 2019 for review of progressive vs multiphase deformation).
- *Folding-and-thrusting* has been invoked in the Karibib District in shallower northeastern portions the southern Central Zone (Kisters et al., 2004). However, typical features of fold-and-thrust belts are not well-developed at the regional-scale in the southern Central Zone: 1) lineations are overwhelmingly orogen-parallel rather than down-dip (Poli and Oliver, 2001; Kruger and Kisetrs, 2016; Jones, 2026), 2) many domes are upright and associated with largely coaxial NW-SE shortening, lacking the consistent vergence direction of fold-thrust belts (Jones, 2026), 3) substantial partial melting and leucogranite magmatism coeval with deformation in the cores of many domes (Figure 10; Jones, 2026) would be expected to restrict the ability of strain to localise into distinct thrusts (Jamieson et al., 2011), and 4) the isobaric heating path to peak HTLP conditions precludes substantial crustal thickening associated with fold-and-thrust stacking (Longridge et al., 2017; Jung et al., 2019; MacRoberts et al., 2025).

- *Cordilleran-style metamorphic core complexes* were invoked by Oliver (1994, 1995). However, the isobaric heating path to peak HTLP conditions (Longridge et al., 2017; Jung et al., 2019; MacRoberts et al., 2025) rules out substantial crustal thinning required for extensional collapse. More recent structural studies also show that c. 530-510 Ma leucogranite dykes (Figure 4) are strongly folded by NE-SW trending fold structures attributed to ongoing NW-SE directed Congo-Kalahari collision (Kruger and Kisters, 2016; Jones, 2026).

5.3.2 Transition to ductile flow in the HTLP Central Zone

Modern thermomechanical models emphasise the role that high-temperature metamorphism can have on the mechanical behaviour of the crust (Jamieson and Beaumont, 2013). Temperatures above 700 ^{O}C lead to widespread partial melting; this can cause the middle crust to become ductile and flow viscously (Jamieson et al., 2011). Tectonic processes in partially molten middle crust can be dominated by *en-masse* ductile flow in response to differential pressure gradients (Figure 1; Jamieson and Beaumont, 2013).

The structural fabric and geometry of the southern Central Zone (Figure 7) appears consistent with *en-masse* ductile flow of partially molten middle crust. Strain is broadly distributed throughout the region (Figure 7), accumulating in a diverse variety of fold structures (Figures 7 and 8), with little to no evidence of strain accumulation along narrow throughgoing faults or shear zones. The structural fabric of the southern Central Zone (Figure 7) contrasts clearly with more linear foreland fold-and-thrust belt fabrics in the Southern and Northern zones (Figure 6).

Field observations document pervasive distributed deformation in migmatitic units in the cores of dome structures in the HTLP southern Central Zone (e.g., Figure 10). Syn-magmatic deformation is further indicated by melt-filled fractures and boudin necks, as well as consistent fold patterns deforming c. 530-510 Ma leucogranite dykes during progressive deformation and magmatism (Kruger and Kiseters, 2016; Jones, 2026). These observations satisfy model predictions that large-scale ductile flow is associated with melt-driven weakening of the mid-crust (Jamieson et al., 2011; Jamieson and Beaumont, 2013).

5.3.3 Style of ductile flow in the HTLP Central Zone

Styles of ductile flow can change in space and time as an orogen evolves, reflecting evolution in crustal thickness, crustal rheology due to partial melting, erosion rates at the orogen flank, and/or changes in the far-field tectonic stresses (Jamieson and Beaumont, 2013). We propose that the observed structural and metamorphic characteristics of the HTLP southern Central Zone are most consistent with an end-member style of ductile flow termed 'lateral constrictional flow' (Figure 11). Lateral constrictional flow can accommodate continued convergence in a mid-crust too weak and gravitationally unstable to sustain further thickening. Instead of thickening the crust, orogen-normal shortening is accommodated by orogen-parallel stretching and lateral extrusion, thereby maintaining isostatic equilibrium (Chardon et al., 2011).

In the southern Central Zone, lateral constrictional flow appears consistent with:

1) The isobaric heating path towards peak HTLP granulite-facies conditions, which indicates that the crust did not substantially thicken or thin at this time (Longridge et al., 2017; Jung et al., 2019; MacRoberts et al., 2025).
2) Widespread orogen-parallel constrictional fabrics, which record NW-SE shortening together with NE-SW orogen-parallel stretching (Poli and Oliver, 2001; Jones, 2026).
3) Field structural relationships which indicate that NW-SE shortening and NE-SW stretching occurred coevally with c. 530-510 Ma leucogranite magmatism (Kruger and Kisters, 2016; Jones, 2026)
4) Geological mapping studies documenting that a Damaran-aged migmatite-granite terrain was likely more extensive throughout the cores of domes than recognised by older studies (see reinterpretations by Oliver and Kinnaird, 1996; Toe et al., 2013; Jones et al., 2026). A widespread migmatite-granite terrain of the sort observed in Figure 10 provides the necessary conditions for a rheologically weak middle-crust capable of undergoing ductile flow (Jamieson et al., 2011).
5) Experimental studies on constrictional deformation document the formation of heterogeneous non-cylindrical fold interference geometries which lack a consistent overprinting relationship (Ghosh et al., 1995). This is consistent with fold geometries observed throughout the southern Central Zone, which contain extremely diverse and inconsistent overprinting relationships varying from one dome to another (Figures 7 and 8; see also Poli, 1997).
6) We speculate that mechanical coupling between neighbouring rock units with strong rheological heterogeneity (Figure 9A-9D) would also contribute to formation of the diverse fold interference structures observed at the regional scale (Figure 7 and 8). This was probably exacerbated by spatial and temporal fluctuations in the volume of melt present in the cores of domes (e.g. Figure

10), which would contribute to substantial variations in crustal rheology between neighbouring mechanically-coupled domes.

Finally, a subordinate component of orogen-parallel sinistral shearing is also recognised by map-scale fabric analysis in the southern Central Zone (Figure 9); its exact timing relative to c. 530-510 Ma leucogranite magmatism and HTLP metamorphism is not precisely constrained, although it certainly occurred after emplacement of the 547+/-7 Ma and 548.5 +/- 5.6 Ma Achas and Gawib plutons, as indicated by deformation of those plutons (Figures 9B and 9C).

5.3.4 Comparison of ductile flow modes to other hot orogens & speculation on the origin of the Donkerhuk Batholith

The observed structural and metamorphic architecture of the deeply eroded southern Central Zone of the Damara Belt does not obviously support imbrication of lower crustal ductile fold nappes in the manner documented from the Canadian Cordillera (Beaumont et al., 2010; Simony and Carr, 2011) or western Grenville Orogen (Jamieson et al., 2007, 2010). Similarly, extrusion of a ductile mid-crustal channel between bounding thrust- and normal-sense shear zones - in the manner observed in the Greater Himalayan Sequence (e.g., Beaumont et al., 2001; Searle et al., 2003; Godin et al., 2006) – has not been documented in the Damara Orogen.

However, the nature of the Donkerhuk Batholith and Okahandja Lineament Zone does warrant further discussion. The Donkerhuk Batholith forms an anomalous high-temperature thermal corridor along the southern flank of the Central Zone, stretching along the boundary with the Southern Zone (Figures 3 and 5). The spatial pattern of the Donkerhuk Batholith – extending along the boundary of the Central and Southern zones (Figure 3) and wrapped by lower-grade metamorphic isograds (Figure 5) – resembles that of the Greater Himalayan Sequence at the southern margin of the Tibetan Plateau (e.g. Beaumont et al., 2001; Searle et al., 2003; Godin et al., 2006). The Donkerhuk Batholith has a mainly peraluminous S-type composition, involving sheet-like emplacement of granitic magmas over ~20-25 Myr from ~535-510 Ma at pressure conditions of ~4.5 kbar. Its most probable source rocks are suggested to be from the Central Zone (Clemens et al., 2017a, 2017b). These characteristics are similar in terms of age, emplacement mechanism, and emplacement depth to the migmatite-granite terrain occurring in the cores of dome structures at deeper levels of the southern Central Zone (Toe et al., 2013; Jones et al., 2026). This poses the question of whether the Donkerhuk Batholith could have been emplaced via SE-directed extrusion of HTLP Central Zone rocks in a manner akin to Himalayan channel flow. Such a hypothesis is speculative at present, since bounding opposite normal- and reverse-sense shear zones which accommodate Himalayan-style channel flow (e.g., Beaumont et al., 2001; Searle et al., 2003; Godin et al., 2006) have not been documented along the margins of the

Donkerhuk Batholith. Clements et al. (2017a) instead interpreted the Donkerhuk Batholith as forming in a fore-arc setting due to underplating of mafic magmas driven by opening of a slab window; however, coeval mafic rocks with mantle geochemical signatures which would directly support this model are also not observed at the current erosion level. Differences in internal architecture and age structure compared to younger fore-arc batholiths were also noted (Clemens et al., 2017b).

5.4 Conceptual hot-orogen evolution for the Damara Orogen

The results of this study suggest that the overall first-order magmatic, metamorphic, and structural architecture of the Damara Belt is well-explained by a conceptual hot-orogen model evolving through the following principal stages (Figure 12):

1. Onset of collision and initial crustal thickening, likely associated with some form of either classical or flat-slab subduction, resulting in intrusion of early c. 575-540 Ma tholeiitic to calc-alkaline magmas (Figure 4).
2. Long-lived radiogenic heat production in the thickened orogenic crust over the following 20-30 Myr, combined with possible heat addition from other sources, substantially raising temperatures in the mid-crust.
3. Attainment of peak HTLP granulite-facies conditions in the Central Zone associated with widespread partial melting and intrusion of c. 530-510 Ma crustal melt leucogranites. This led to strong deformation partitioning between ductile flow in the Central Zone and foreland-vergent folding-and-thrusting in the external LTHP wedges (Figures 11 and 12).

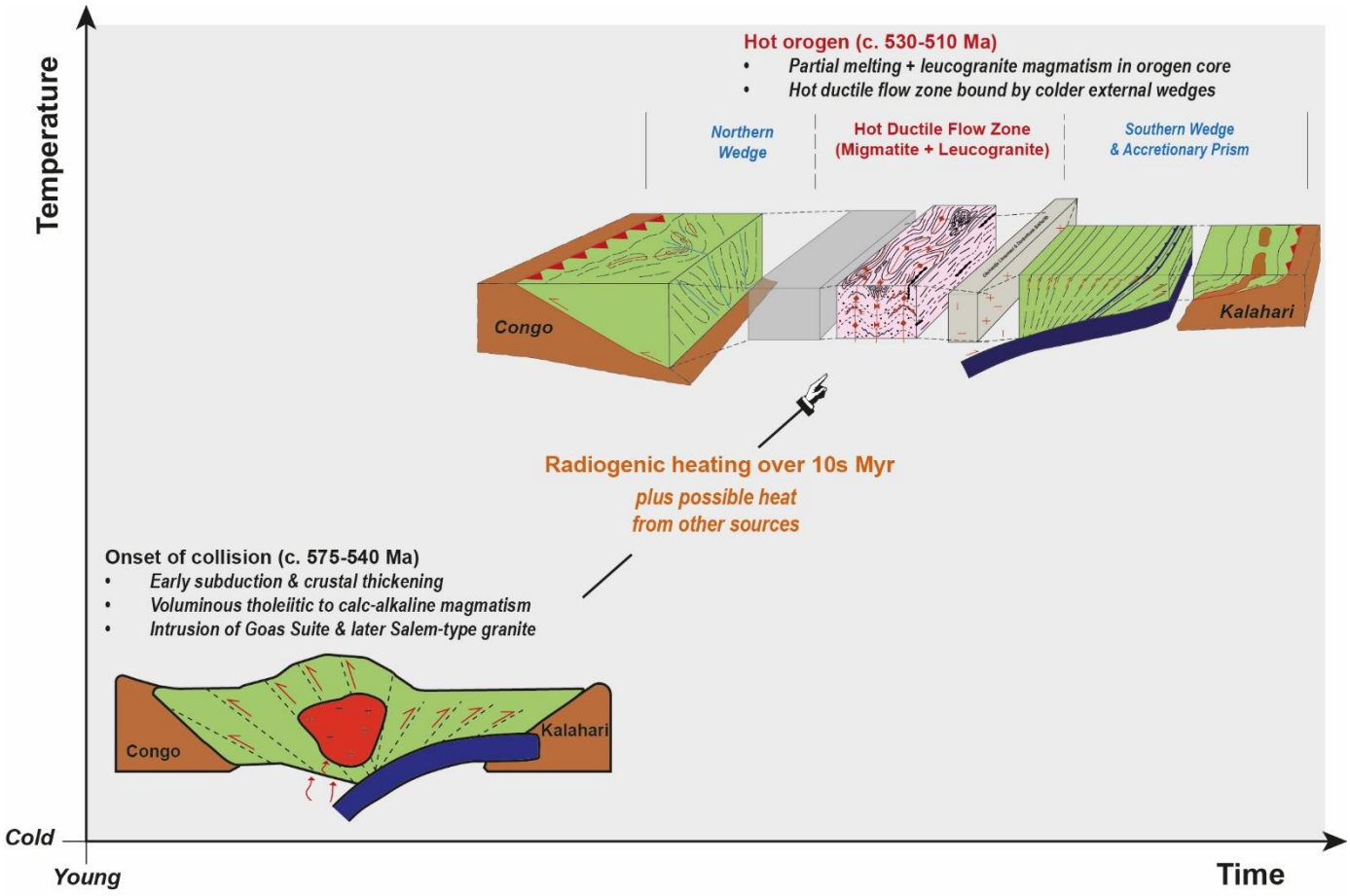

Figure 12 – Schematic temperature-time chart illustrating the conceptual evolution of a hot orogen in the Damara Belt.

5.5 Unresolved questions

5.5.1 A small-hot orogen?

The Damara Belt is unusually hot considering its modest magnitude; its maximum across-strike width of ~600-700 km is far smaller than the 1,500-2,000 km width of the Himalaya-Tibet system. Similarly, maximum documented pressure conditions of ~8-11.5 kbar in the Damara Belt (Goscombe et al., 2017b) are lower than that of the Himalaya-Tibet system and indicate a thinner crust. The conceptual model of Jamieson and Beaumont (2013) links temperature to magnitude as a first-order approximation, noting that bigger, thicker, orogens tend to be hotter. However, the Damara Orogen shows that smaller, thinner, belts can also obtain high temperatures.

Potential causes of unusually high temperatures in the Damara Belt may include 1) unusually high concentrations of heat-producing elements deposited in Damaran metasedimentary units, 2) the widespread intrusion of earlier tholeiitic to calc-alkaline magmas potentially contributing significant heat and also further enhancing the concentration of radioactive heat producing elements in the crust, 3) long-timeframes of collision allowing more time for radioactive heat production, 4) lower erosion rates which could help to insulate heat, and 5) potential thinning of the lithosphere which may increase basal heat flow from the mantle.

5.5.2 Quantifying the contribution of heat from different sources in the HTLP Damara Belt

Radiogenic heat production is likely to be the baseline driver of HTLP metamorphism in orogenic belts (Clark et al., 2011; Jamieson and Beaumont, 2013; Kelsey and Hand, 2015; Jiao et al., 2023). The extent of radiogenic heat production in the Damara Belt could be estimated from the concentration of heat producing elements in Damaran metasedimentary units, as well as in c. 575-540 Ma tholeiitic to calc-alkaline plutons emplaced into the Central Zone at an earlier stage of the orogen's evolution. Timeframes of collision and estimates of crustal thickness are available from published igneous rock ages (Figure 4) and metamorphic analyses (Longridge et al., 2017; Jung et al., 2019; MacRoberts et al., 2025). If a gap is observed between estimated total radiogenic heat production and the actual observed regional metamorphic temperatures of 800^{O}C, this provides quantitative evidence indicating the requirement for heat from other sources such as the mantle.

5.5.3 Varying tectonic style along strike in the Damara-Lufilian-Zambezi orogenic belt

An additional unresolved question concerns along-strike variations in tectonic style observed between the HTLP Damara Belt and the low-temperature but high/ultra-high pressure Zambezi Belt (Figure 2; Goscombe et al., 2020). It may be significant that peak HTLP regional metamorphic conditions in the Damara Belt occur in the southwestern Central Zone (Figure 5), near to the triple junction intersection with the Kaoko and Gariep Belts (Figure 2). A potential role for this complex triple junction in the attainment of HTLP conditions has not been investigated. However, investigation is complicated by opening of the South Atlantic Ocean, which split the rock record of Congo-Kalahari-Rio de la Plata craton collision into the Damara, Kaoko and Gariep belts in Namibia, and the Dom Feliciano Belt in South America (Figure 2). Another potential explanation may be the existence of a thicker and wider portion of oceanic crust separating the Congo and Kalahari cratons further east, as suggested by exhumation of ultra-high pressure eclogites in the Zambezi Belt (John et al., 2003, 2004) - deep subduction may trigger cold rather than hot orogenic behaviour (Fossen et al., 2017). Additional factors may include variations in the concentration of radioactive elements in the inverted metasedimentary basin, different convergence rates and durations of collision along strike, possible enhanced mantle heat flow in the Damara Belt, and/or differing erosion rates preserving or removing thickened orogenic crust.

6) Conclusions

1. **The Damara Belt preserves the first-order architecture of a hot collisional orogen**

   The orogen is strongly partitioned between a high-temperature, low-pressure (HTLP) Central Zone and lower-temperature, higher-pressure (LTHP) Northern and Southern zones. The Central Zone is characterised by Buchan-series metamorphism, widespread granite–migmatite terranes, voluminous crustally derived granites, and complex regional fold interference patterns. Meanwhile, the flanking zones preserve comparatively linear fabrics, inverted Barrovian metamorphic gradients, and foreland-vergent fold-and-thrust wedge geometries.

2. **Signature of radiogenic heating driving HTLP metamorphism**

   Igneous rocks record early calc-alkaline to tholeiitic magmatism at ca. 575–540 Ma, followed by widespread leucogranite magmatism at ca. 530–510 Ma. The 20–30 Myr delay between early magmatism and peak crustal melting is characteristic of long-lived radiogenic heat production. Possible additional heat contributions from mantle-derived heat and/or earlier magmatic emplacement need further quantification.

3. **Temperature controls deformation style during collision**

   The contrast between distributed, heterogeneous deformation in the HTLP Central Zone and wedge-dominated contractional structures in the cooler marginal zones demonstrates the role that temperature has on mechanical behaviour. These relationships indicate that progressive heating and partial melting can fundamentally transform the structural style and tectonic response to ongoing continent-continent collision.

4. **3-dimensinoal complexity of ductile flow in hot orogens**

   Structural relationships in the HTLP southern Central Zone are most consistent with 3-dimensional ductile flow within a weak, partially molten mid-crust. Deformation combined NW–SE shortening, subhorizontal NE–SW orogen-parallel stretching, and subordinate orogen-parallel sinistral shearing in a lateral constrictional flow regime; this acted to maintain a consistent crustal thickness during continued convergence. The structural complexity of the Central Zone, including strong spatial variations in fold style and rheological behaviour, is difficult to fully capture in end-member two-dimensional wedge or channel-flow models. Instead, the Damara Belt demonstrates that deformation in hot orogens can be inherently three-dimensional, strongly influenced by lithological heterogeneity, evolving melt fraction, and mechanical coupling between neighbouring rock volumes with heterogeneous compositions and diverse rheological behaviours.

5. Broader implications

The Damara Orogen provides a well-exposed natural analogue for thermally weakened collisional systems. It shows that hot-orogen style behaviour is not restricted to the largest plateau-forming belts; under favourable thermal conditions, even moderately sized orogens may undergo major transitions from contractional wedge tectonics to distributed ductile flow in their mid-crustal interiors.

7) Acknowledgements

This work forms part of T. Jones' PhD research. The support of the DST-NRF Centre of Excellence for Integrated Mineral and Energy Resource Analysis (DST-NRF CIMERA) towards this research is acknowledged. Additional support from the Society of Economic Geologists (SEG) in the form of a Graduate Student Fellowship and a Student Research Grant from the McKinstry Fund is greatly appreciated. Deep Yellow Ltd and Reptile Mineral Resources are thanked for contributing towards the PhD funding of T. Jones, providing logistical support during fieldwork, and providing access to regional satellite and aeromagnetic datasets used in this analysis. Opinions expressed and conclusions arrived at are solely those of the authors; they may not reflect the opinions or conclusions of the supporting bodies.

8) Appendix

Table 1 – Compilation of igneous rock ages for the Central Zone of the Damara Orogen.

	Source	Rock Type (Simplified)	Age (Ma)	Error range (+/- Myr)	Age dating method
1	Allsopp et al. 1983	Salem granite	580	30	U-Pb TIMS
2	Bergemann et al., 2014	Granodiorite-granite	576.2	5.7	U-Pb zircon
3	Wits RTX project 2011-2013 (see Milani et al 2015)	Metagabbro	573	9	U-Pb LA-SF-ICP-MS
4	Bergemann et al., 2014	Granodiorite-granite	570.9	4.9	U-Pb zircon
5	Wits RTX project 2011-2013 (see Milani et al 2015)	Metagabbro	570	6	U-Pb LA-SF-ICP-MS
6	Jung et al., 2020	Quartz monzonite	569.3	3	U-Pb zircon
7	Wits RTX project 2011-2013 (see Milani et al 2015)	Diorite	569	8	U-Pb LA-SF-ICP-MS
8	Wits RTX project 2011-2013 (see Milani et al 2015)	Diorite	568	3	U-Pb LA-SF-ICP-MS
9	Wits RTX project 2011-2013 (see Milani et al 2015)	Metagabbro	567	7	U-Pb LA-SF-ICP-MS
10	Wits RTX project 2011-2013 (see Milani et al 2015)	Granodiorite	566	10	U-Pb LA-SF-ICP-MS
11	Jung et al. 2020	Granodiorite	563.7	6.1	U-Pb zircon
12	Jacob et al. 2000	Quartz Diorite	563	4	U-Pb SHRIMP
13	Wits RTX project 2011-2013 (see Milani et al 2015)	Diorite	562	6	U-Pb LA-SF-ICP-MS
14	Wits RTX project 2011-2013 (see Milani et al 2015)	Granite	562	8	U-Pb LA-SF-ICP-MS
15	De Kock et al. 2000	Diorite	558	5	U-Pb SHRIMP
16	Wits RTX project 2011-2013 (see Milani et al 2015)	Quartz-monzonite	558	8	U-Pb LA-SF-ICP-MS
17	Wits RTX project 2011-2013 (see Milani et al 2015)	Monzonite	557	10	U-Pb LA-SF-ICP-MS
18	Kroner (1982)	Salem granite	554	17	Rb-Sr whole rock
19	Downing (1982)	Salem granite	554	33	Rb-Sr whole rock
20	Ostendorf et al (2014)	Grey granite	553.3	8.4	U-Pb LA-ICP-MS
21	Johnson et al. (2006)	Salem granite	549	11	U-Pb LA-ICP-MS
22	Osterhus et al. 2014	Granodiorite	548.5	5.6	U-Pb zircon
23	Jung et al., 2020	Syenite	548	12	LA-ICP-MS U-Pb zircon
24	Simon et al., 2017	Granodiorite	547	7	U-Pb zircon
25	Jacob et al. 2000	Quartz Diorite	546	6	U-Pb SHRIMP
26	Jacob et al. 2000	Rotekuppe monzogranite	543	5	U-Pb SHRIMP
27	Jung et al., 2020	Monzonite	542.2	7	LA-ICP-MS U-Pb zircon
28	Tack et al 2002	Grey granite	542	6	U-Pb zircon
29	Jung et al., 2014	Quartz diorite	541	3	LA-ICP-MS U-Pb zircon
30	Jacob et al. 2000	Rotekuppe monzogranite	539	6	U-Pb SHRIMP
31	Longridge et al 2011	Red granite	539	17	SHRIMP U-Pb zircon and/or monazite
32	Wits RTX project 2011-2013 (see Milani et al 2015)	Salem granite	539	6	U-Pb LA-SF-ICP-MS
33	Goslin (2019)	Red granite	535.77	0.96	U-Pb zircon
34	Briquet et al 1980	Red granite	534	7	U-Pb monazite
35	Jung and Mezger 2003	Leucogranite	530	3	Sm-Nd garnet
36	Tack et al 2002	Grey granite	526	17	U-Pb zircon
37	Goslin (2019)	Leucogranite	525.72	1.91	U-Pb zircon
38	Longridge et al 2011	Grey granite	520.4	4.2	SHRIMP U-Pb zircon and/or monazite
39	Longridge et al 2017	Leucogranite	520.3	4.6	U-Pb single-grain zircon
40	Jung et al. 2001	Leucogranite	517	2	U-Pb monazite
41	Longridge et al 2017	Leucogranite	514.1	3.1	U-Pb single-grain monazite
42	Longridge et al 2011	Leucogranite	511	18	SHRIMP U-Pb zircon and/or monazite
43	Jung et al. 2001	Leucogranite	511	2	U-Pb monazite
44	Jung and Mezger 2003	Leucogranite	510	2	Sm-Nd garnet
45	Jung and Mezger 2003	Leucogranite	509	5	Sm-Nd garnet
46	Briquet et al 1980	Leucogranite	509	1	Concordant uraninite
47	Longridge et al 2011	Leucogranite	508.4	8.7	SHRIMP U-Pb zircon and/or monazite
48	Briquet et al 1980	Leucogranite	508	2	Concordant monazite
49	Paul et al., 2014	Leucogranite	508	5.9	U-Pb ID-TIMS Monazite
50	Jung et al., 2014	Granodiorite	506	6	LA-ICP-MS U-Pb zircon
51	Ostendorf et al (2014)	Leucogranite	502.4	9	U-Pb LA-ICP-MS
52	Jung and Mezger 2003	Leucogranite	469	10	Sm-Nd garnet
53	Jung and Mezger 2003	Leucogranite	469	3	Sm-Nd garnet

9) References

Allsopp, H. L., Barton, E. S., Kröner, A., Welke, H. J. & Burger, A. J. (1983). Emplacement versus inherited isotopic age patterns: a Rb-Sr and U-Pb study of Salem-type granites in the central Damara Belt. In: Miller, R. McG. (Ed.) Evolution of the Damara Orogen. *Special Publications of the Geological Society of South Africa*, **11**, 281-287.

Ashworth, L., Kinnaird, J.A., Nex, P.A.M., Harris, C. and Müller, A., 2020. Origin of rare-element mineralized Damara Belt pegmatites: a geochemical and light stable isotope study. *Lithos*, 372–373, 105655.

Barnes, J.F.H. and Downing, K.N. 1979. Origin of domes in the central Damara belt, Namibia. *Rev. Geol. Dynam. Geogr. Phys. 21, 383-386*.

Barnes, J.F.H., 1981. Some aspects of the tectonic history of the Khan-Swakop region of the Damara Belt, Namibia. *Unpublished PhD thesis, University of Leeds, United Kingdom*.

Beaumont, C., Muñoz, J.A., Hamilton, J., and Fullsack, P., 2000. Factors controlling the Alpine evolution of the central Pyrenees inferred from a comparison of observations and geodynamical models: *Journal of Geophysical Research*, v. 105, p. 8121–8145, doi:10.1029 /1999JB900390.

Beaumont, C., Jamieson, R.A., Nguyen, M.H., Lee, B., 2001. Himalayan tectonics explained by extrusion of a low-viscosity crustal channel coupled to focused surface denudation. *Nature* 414, 738 – 742.

Beaumont, C., Nguyen, M.H., Jamieson, R.A., and Ellis, S., 2006, Crustal flow modes in large hot orogens, in Law, R.D., Searle, M.P., and Godin, L., eds., Channel Flow, Ductile Extrusion and Exhumation of Lower Mid-Crust in Continental Collision Zones: *Geological Society of London Special Publication* 268, p. 91–145.

Beaumont, C., Jamieson, R.A., and Nguyen, M.H., 2010, Models of large, hot orogens containing a collage of reworked and accreted terranes: *Canadian Journal of Earth Sciences*, v. 47, p. 485–515.

Bergemann, C., Jung, S., Berndt, J., Stracke, A., Hauff, F., 2014. Generation of magnesian, high-K alkali-calcic granites and granodiorites from amphibolitic continental crust in the Damara orogen, Namibia. *Lithos* **198–199**, 217–233.

Buiter, S. J. H. 2012. A review of brittle compressional wedge models, *Tectonophysics, 530–531, 1–17*.

Brandt, R. 1987. A revised stratigraphy for the Abbabis Complex in the Abbabis Inlier, Namibia. *South African Journal of Geology*. **90**, 314-323

Briqueu, L., Lancelot, J.R., Valois, J.-P., Walgenwitz, F., 1980. Gdochronologie U-Pb et genese d'un type de mineralisation uranifere: Les alaskites de Goanikontes (Namibie) et leur encaissant. *Bulletin Centres Recherches Exploration Production Elf, Aquitaine* **4**, 759-811.

Chardon, D., Jayananda, M., Peucat, J.J., 2011. Lateral constrictional flow of hot orogenic crust: Insights from the Neoarchean of South India, geological and geophysical implications for orogenic plateaux. *G3 – Geochemistry, Geophysics, Geosystems 12 (Q02005), http://dx.doi.org/10.1029/2010GC003398*.

Clark, M.K., and Royden, L.H., 2000, Topographic ooze: Building the eastern margin of Tibet by lower crustal flow: *Geology*, v. 28, p. 703–706, doi:10

Clark, C., Fitzsimons, I.C.W., Healy, D., Harley, S.L., 2011, How does the continental crust get really hot? *Elements, 7 (4), 235-240*

Clemens JD, Buick IS, Kisters AFM, Frei D. 2017. Petrogenesis of the granitic Donkerhuk batholith in the Damara Belt of Namibia: protracted, syntectonic, short-range, crustal magma transfer. *Contrib to Mineral Petrol* 172:1–23. https:// doi. org/ 10. 1007/s00410-017-1370-0

Clemens, J. D., Buick, I. S., & Kisters, A. F. M. 2017. The Donkerhuk batholith, Namibia: A giant S-type granite emplaced in the mid crust, in a fore-arc setting. *Journal of the Geological Society*, 174(1), 157–169. https://doi.org/10.1144/jgs2016-028

Clemens, J.D., Kisters, A.F.M. 2021. Magmatic indicators of subduction initiation: The bimodal Goas intrusive Suite in the Pan-African Damara Belt of Namibia. *Precambrian Research*. **362**. https://doi.org/10.1016/j.precamres.2021.106309

Clemens, J.D., 2022. Mingling with minimal mixing: mafic-silicic magma interactions in the Oamikaub ring complex, Namibia. *J. Afr. Earth Sci*. 193, 104602

Dahlen, F. A., 1990. Critical taper model of fold-and-thrust belts and accretionary wedges, *Annu. Rev. Earth Planet. Sci., 18, 55–99.*

De Kock, G. S., Eglington, B., Armstrong, R. A., Harmer, R. E. & Walraven, F. (2000). U-Pb and Pb-Pb ages of the Naauwpoort rhyolite, Kawaeup leptite and Okongava diorite: implications for the onset of rifting and orogenesis in the Damara belt, Namibia. *Communication of the Geological Survey of Namibia*, **12**, 81-88.

Downing, K. N. (1982). The evolution of the Okahandja Lineament and its significance for Damara tectonics in Namibia. *Unpublished PhD thesis, University of Leeds, United Kingdom*.

Eskola, P.E., 1949, The problem of mantled gneiss domes: *Geological Society of London, Quarterly Journal, v. 104, p. 461–476.*

Fossen, H., Cavalcante, G.C., de Almeida, R.P., 2017. Hot versus cold orogenic behavior: Comparing the Aracuaı-West Congo and the Caledonian Orogens. *Tectonics* 36, 2159–2178.1688 doi:10.1002/2017tc004743

Fossen, H., Cavalcante, G. C. G., Pinheiro, R. V. L., & Archanjo, C. J. (2019). Deformation—Progressive or multiphase? *Journal of Structural Geology*, **125**, 82–99. https://doi.org/10.1016/j.jsg.2018.05.006

Frimmel H.E. 2008. The Gariep Belt. In: Miller RM (ed) *The geology of Namibia.* Geological Survey of Namibia, Windhoek, pp 14-11–14-39

Ghosh, S. K., Khan, D., & Sengupta, S. (1995). Interfering folds in constrictional deformation. *Journal of Structural Geology*, 17(10), 1361–1373. https://doi.org/10.1016/0191 8141(95)00027-B

Godin, L., Grujic, D., Law, R.D., Searle, M.P., 2006. Channel flow, ductile extrusion and exhumation in continental collision zones: an introduction. *Geol. Soc. Spec. Publ. 268, 1–23. http://dx.doi.org/10.1144/GSL.SP.2006.268.01.01.*

Goscombe B, Foster DA, Gray D, Wade B, Marsellos A, Titus J. 2017a. Deformation correlations, stress field switches and evolution of an orogenic intersection: the Pan-African Kaoko-Damara orogenic junction, Namibia. *Geosci Front* 8(6):1187–1232. https://doi.org/10.1016/j.gsf.2017.05.001

Goscombe, B., Foster, D. A., Gray, D., & Wade, B. 2017b. Metamorphic response and crustal architecture in a classical collisional orogen: The Damara Belt, Namibia. *Gondwana Research*, **52**, 80– 124. https://doi.org/10.1016/j.gr.2017.07.006

Goscombe, B., Foster, D.A., Gray, D., Wade, B., 2020. Assembly of central Gondwana along the Zambezi Belt: Metamorphic response and basement reactivation during the Kuunga Orogeny. *Gondwana Research* 80, 410–465. doi:10.1016/j.gr.2019.11.004.

Goslin, L.M., 2019. Deformation and partial melting in the Central Zone of the Damara Orogen, Namibia. *Unpublished Ph.D. thesis, University of the Witwatersrand*.

Gray, D.R., Foster, D.A., Meert, J.G., Goscombe, B.D., Armstrong, R., Trouw, R.A.J., Passchier, C.W., 2008. A Damara Orogen perspective on the assembly of southwestern Gondwana. In: Pankhurst, R.J., Trouw, R.A.J., De Brito Neves, B.B., De Wit, M.J. (Eds.), West Gondwana: Pre-Cenozoic Correlations Across South Atlantic Region. Geological *Society London Special Publication*, 294, pp. 257–278

Haack, U., Gohn, E., Hartmann, O., 1983. Radiogenic heat generation in Damaran rocks, in: *Miller, R.McG. (Ed.), Evolution of the Damara Orogen of South West Africa/Namibia. Geol. Soc. South Africa, Spec. Publ*. 11, 225-232

Hars, E.M., Jung, S., Romer, R.L. 2025. Petrogenesis of the synorogenic alkaline Doros intrusion: Insights into geodynamic processes and lithospheric mantle heterogeneity beneath the Damara belt, Namibia. *Lithos*. 514-515. https://doi.org/10.1016/j.lithos.2025.108192

Hartmann, O., Hoffer, E., Haack, U., 1983. Regional metamorphism in the Damara orogen: Interaction of crustal motion and heat transfer. *Geol. Soc. S. Afr. Spec. Publ*. 11, 233–241.

Hartnady, M.I.H. 2014. The structural evolution of an ancient accretionary prism in the Damara Belt, Namibia. *Unpublished MSc thesis, University of Cape Town, South Africa.*

Henry, G. 1992. The sedimentary evolution of the Damara Sequence in the lower Khan River valley, Namibia. *Ph.D. thesis (unpubl.), University Witwatersrand*, 217p

Jacob, R.E., Snowden, P.A., Bunting, F.J.L., 1983. Geology and Structural development of the Tumas basement dome and its cover rocks. In: Miller, R.McG. (Ed.), Evolution of the Damara Oroqen of South West Africa/Namibia. *Geological Society of South Africa, Special Publication* **11**, pp. 409-421.

Jacob, R. E., Moore, J. M. & Armstrong, R. A. (2000). Zircon and Titanite age determination from igneous rocks in the Karibib District, Namibia: implications for Navachab vein-style gold mineralization. *Communication of the Geological Survey of Namibia*, **12**, 157-166.

Jamieson, R. A., and C. Beaumont (2013), On the origin of orogens, *Geological Society of America Bulletin*. **125 (11-12)**, 1671–1702

Jamieson, R.A., Beaumont, C., Nguyen, M.H., and Culshaw, N.G., 2007, Synconvergent ductile flow in variable strength continental crust: Numerical models with application to the western Grenville orogen: *Tectonics*, v. 26, TC5005, doi:10.1029/2006TC002036.

Jamieson, R.A., Beaumont, C., Warren, C.J., and Nguyen, M.H., 2010, The Grenville orogen explained? Applications and limitations of integrating numerical models with geological and geophysical data: *Canadian Journal of Earth Sciences*, v. 47, p. 517–539, doi:10.1139/E09-070.

Jamieson, R.A., Unsworth, M.J., Harris, N.B.W., Rosenberg, C.L. & Schulmann, K. 2011. Crustal melting and the flow of mountains. *Elements*, **7**, 253–260.

Jiao, S., Brown, M., Mitchell, R.N., Chowdhury, P., Clark, C., Chen, L., Chen, Y., Korhonen, F., Huang, G., Guo, J. 2023. Mechanisms to generate ultrahigh-temperature metamorphism. *Nat. Rev. Earth Environ*. 4, 298–318

John, T., Schenk, V., Haase, K., Scherer, E., Tembo, F., 2003. Evidence for a Neoproterozoic ocean in south-central Africa from mid-oceanic-ridge-type geochemical signatures and pressure-temperature estimates of Zambian eclogites. *Geology* 31, 243–246.

John, T., Schenk, V., Mezger, K., Tembo, F., 2004. Timing and PT evolution of whiteschist metamorphism in the Lufilian Arc-Zambezi Belt Orogen (Zambia); implications for the assembly of Gondwana. *J. Geol.* 112, 71–90.

Johnson, S. D., Poujol, M. & Kisters, A. F. M. (2006). Constraining the timing and migration of collisional tectonics in the Damara Belt, Namibia: U-Pb zircon ages for the syntectonic Salem-type Stinkbank granite. *South African Journal of Geology*, **109**, 611-624.

Jones, T.L., Otto, A., Becker, E., Wilde, A. 2026. Reevaluating the Abbabis Complex: Intrusive relationships and melt connectivity in a syn-orogenic migmatite–granite system, Damara Orogen, Namibia. *Preprint at eartharxiv*: https://doi.org/10.31223/X5MR2B

Jones, T.L. 2026. Structural & tectonic setting of pegmatite dykes in the Damara Orogen, Namibia. *Unpublished PhD research report, University of the Witwatersrand, South Africa*. 10.13140/RG.2.2.34493.52961

Jung, S. & Mezger, K. 2001. Geochronology in migmatites – a Sm–Nd, U–Pb and Rb–Sr study from the Proterozoic Damara belt (Namibia): implications for polyphase development of migmatites in high-grade terranes. *Journal of Metamorphic Geology*, 19, 77–97.

Jung, S. & Mezger, K. (2003). Petrology of basement-dominated terranes: I. Regional metamorphic T-t path and geochronological constraints on Pan-African high-grade metamorphism (central Damara orogen, Namibia). *Chemical Geology*, **198**, 223-247.

Jung, S., and Hauff, F., 2021, Petrogenesis of a low-87Sr/86Sr, two-mica, garnet-bearing leucogranite (Donkerhoek batholith, Damara orogen, Namibia): *Journal of African Earth Sciences*, v. 174, https://doi.org/10.1016/j .jafrearsci .2020 .104055.

Jung, S., Romer, R.L., 2024. The early syn-tectonic mafic to felsic Oamikaub Ring complex (Damara orogen, Namibia) revisited – no role for a Pacific-type subduction? *Prec. Res*. 414, 107612.

Jung, S., Hoffer, E., Masberg, P. and Hoernes, S., 1995. Geochemistry of granitic in-situ low-melt fractions – an example from the Central Damara Orogen. *Communications of the Geological Survey of Namibia*, 10, pp.21–32.

Jung, S., Hoernes, S. and Mezger, K., 2001. Trace element and isotopic (Sr, Nd, Pb, O) arguments for a mid-crustal origin of Pan-African garnet-bearing S-type granites from the Damara orogen (Namibia). *Precambrian Research*, 110, pp.325–355.

Jung, C., Jung, S., Nebel, O., Hellebrand, E., Masberg, P. and Hoffer, E., 2009. Fluid-present melting of meta-igneous rocks and the generation of leucogranites – Constraints from garnet major- and trace element data, Lu–Hf whole rock–garnet ages and whole rock Nd–Sr–Hf–O isotope data. *Lithos*, 111, pp.220–235.

Jung, S., Berndt, J., Stracke, A., Hauff, F., Kastek, N., 2014. Anatexis of juvenile mafic to intermediate crust – constraints from major and trace element and Sr, Nd, Pb isotopes of diorites to granites (Damara orogen, Namibia). *South African Journal of Geology*. **117**, 149–171.

Jung, S., Brandt, S., Bast, R., Scherer, E.E., Berndt, J., 2019. Metamorphic petrology of a high-T/low-P granulite terrane (Damara belt, Namibia) – constraints from pseudosection modelling and high-precision Lu-Hf garnet-whole rock dating. *Journal of Metamorphic Geology*. **37 (1)**, 41–69. https://doi.org/10.1111/jmg.2019.37.issue- 110.1111/jmg.12448.

Jung, S., Pfander, J.A., Hauff, F., Berndt, J., 2020a Crust-mantle interaction during syn- collisional magmatism – Evidence from the Oamikaub diorite and Neikhoes metagabbro (Damara orogen, Namibia). *Precambrian Research*. **351**, https://doi.org/10.1016/j.precamres.2020.105955.

Jung, S., Hauff, F., & Berndt, J. 2020b. Generation of a potassic to ultrapotassic alkaline complex in a syn-collisional setting through flat subduction: Constraints on magma sources and processes (Otjimbingwe alkaline complex, Damara orogen, Namibia). *Gondwana Research*, **82**, 267–287.

Jung, S., Romer, R.L., Pfander, J.A., Berndt, J., 2020c. Petrogenesis of early syn-tectonic monzonite-granodiorite complexes – Crustal reprocessing versus crustal growth. *Precambrian Research*. **351**, 105957. https://doi.org/10.1016/j.precamres.2020.105957.

Jung, S., Mezger, K., Scherer, E.E., Pfander, J.A., Brandt, S., Hellebrand, E. 2026. Petrochronology of a high-temperature granulite terrane – the Damara orogen (Namibia). Gondwana Research. 156, 117-140. https://doi.org/10.1016/j.gr.2026.02.012

Kelsey, D.E., Hand, M. 2015. On ultrahigh temperature crustal metamorphism: Phase equilibria, trace element thermometry, bulk composition, heat sources, timescales and tectonic settings. *Geosci. Front*. 6, 311–356.

Kisters, A.F.M., Jordaan, L.S., Neumaier, K., 2004. Thrust-related dome structures in the Karibib district and the origin of orthogonal fabric domains in the south Central Zone of the Pan-African Damara belt, Namibia. *Precambrian Research 133, 283-303.*

Kitt S, Kisters A, Steven N, Maiden K, Hartmann K (2016) Shear-zone hosted copper mineralisation of the Omitiomire deposit—structural controls of fluid flow and mineralisation during subduction accretion in the Pan-African Damara Belt of Namibia. *Ore Geol Rev* 75:1–15

Kitt, S., Kisters, A., Buick, I and Kramers, J. 2018. Structural, Geochronological and P-T Constraints on Subduction-Accretion Processes in a Pan-African Accretionary Wedge—The Deep Level Southern Zone of the Damara Belt in Namibia. *Precambrian Research 310: 39–62.*

Knupp, K.P. 2019. Regional Airborne Geophysical Interpretation, Uranium Province, Western Namibia. *Internal report produced on behalf of Reptile Mineral Resources, Swakopmund, Namibia*.

Kroner, A. (1982). Rb-Sr geochronology and tectonic evolution of the Pan-African Damara belt of Namibia, southwestern Africa. *American Journal of Science*, **282**, 1471-1507.

Kroner, A. (1984), Dome structures and basement reactivation in the Pan-African Damara belt of Namibia, in *Precambrian Tectonics Illustrated*, edited by A. Kroner and R. Greiling, pp. 191 – 206, *E. Schweizerbart'sche, Stuttgart, Germany*.

Kruckenberg, S.C., Vanderhaeghe, O., Ferré, E.C., Teyssier, C., Whitney, D.L., 2011. Flow of partially molten crust and the internal dynamics of a migmatite dome, Naxos, Greece. *Tectonics* 30, TC3001, doi:10.1029/2010TC002751.

Kruger, T., Kisters, A., 2016. Magma accumulation and segregation during regional-scale folding: the Holland's dome granite injection complex, Damara belt, Namibia. *Journal of Structural Geology* http://dx.doi.org/10.1016/j.jsg.2016.05.002.

Kukla P.A. and Stanistreet I.G., 1991. Record of the Damaran Khomas Hochland accretionary prism in central Namibia: Refutation of an “ensialic” origin of a Late Proterozoic orogenic belt. *Geology*, **19**: 473-476.

Lehmann, J., Saalmann, K., Naydenov, K.V., Milani, L., Belyanin, G.A., Zwingmann, H., Charlesworth, G., Kinnaird, J.A., 2016. Structural and geochronological constraints on the Pan-African tectonic evolution of the northern Damara Belt, Namibia. *Tectonics 35 (1), 103–135.*

Lehtonen, M.I., Manninen, T.E.T. and Schreiber, U.M. (1996). Report: lithostratigraphy of the area between the Swakop, Khan and lower Omaruru Rivers, Namib Desert. *Geological Survey of Namibia Communications*, **11**, 65–75.

Longridge, L., Gibson, R.L., Kinnaird, J.A. and Armstrong, R.A., 2011. Constraining the timing of deformation in the southwestern Central Zone of the Damara Belt, Namibia. In: D.J.J. Van Hinsbergen, S.J.H. Buiter, T.H. Torsvik, C. Gaina and S.J. Webb (Editors), The Formation and Evolution of Africa: A Synopsis of 3.8 Ga of Earth History. *Geological Society, London, Special Publications*, **357**, 107–135.

Longridge, L., Gibson, R.L., Kinnaird, J.A. and Armstrong, R.A., 2017. New constraints on the age and conditions of LPHT metamorphism in the southwestern Central Zone of the Damara Belt, Namibia and implications for tectonic setting. *Lithos* , 278-281, 361–382. doi: 10.1016/j.lithos.2017.02.006

Longridge, L., Kinnaird, J.A., Gibson, R., Hawkesworth, C., Armstrong, R., 2018. Crystal recycling in the Damara Belt, Namibia, and interaction of the Congo and KalahariCratons–evidence from zircon U–Pb, Hf and O isotopes. *South African Journal of Geology*. **121 (3)**,237–252.

Longridge, L., 2012. Tectonothermal Evolution of the Southwestern Central Zone, Damara Belt, Namibia. *Unpublished Ph.D. thesis, University of the Witwatersrand, South Africa* (522 pp.).

MacRoberts, R.J. 2025. Polyphase deformation during prolonged high-temperature, low-pressure metamorphism: An example from the Namibfontein-Vergenoeg migmatite domes, Central Zone, Damara Belt, Namibia. *Journal of Metamorphic Geology*. 0. 1-35.

Marlow, A.G., 1981. Remobilisation and primary uranium genesis in the Damaran Orogenic Belt, Namibia. *Unpublished PhD thesis, University of Leeds, United Kingdom*.

Meneghini, F., A. Kisters, I. Buick, and Å. Fagereng (2014), Fingerprints of late Neoproterozoic ridge subduction in the Pan–African Damara belt, Namibia, *Geology, doi:10.1130/g35932.1.*

Meneghini, F., Fagereng, A. and Kisters, A., 2017. The Matchless Amphibolite of the Damara belt, Namibia: unique preservation of a late Neoproterozoic ophiolitic suture. Ofioliti , 42, 129–145., doi:10.4454/ofioliti.v42i2.452

Merdith, A.S., Collins, A.S., Williams, S.E., Pisarevsky, S., Foden, J.D., Archibald, D.B., Blades, M.L., Alessio, B.L., Armistead, S., Plavsa, D., Clark, C., Müller, R.D., 2017a. A full-plate global

reconstruction of the Neoproterozoic. *Gondwana Res*. 50, 84–134.2586 https://doi.org/10.1016/j.gr.2017.04.001

Milani, L., Kinnaird, J.A., Lehmann, J., Naydenov, K.V., Saalmann, K., Frei, D., Gerdes, A., 2015. Role of crustal contribution in the early stage of the Damara Orogen, Namibia: new constraints from combined U-Pb and Lu-Hf isotopes from the Goas Magmatic Complex. *Gondwana Research*. **28**, 961–986.

Miller, R. 1983. The Pan-African Damara Orogen of South West Africa/Namibia. *Evolution of the Damara orogen of South West Africa/Namibia: Geological Society of South Africa Special Publication*, 11. 431-515

Miller, R. McG. & Grote, W. 1988. Geological Map of the Damara orogen, Namibia (scale 1:500,000). *Geological Survey of Namibia, Windhoek*.

Miller R. McG., 2008. The geology of Namibia, Vol. 2: Neoproterozoic to Lower Paleocene. *Geol. Survey Namibia, Windhoek. Namibia*.

Nabelek, P.I., Whittington, A.G., and Hofmeister, A.M., 2010, Strain heating as a mechanism for partial melting and ultrahigh temperature metamorphism in convergent orogens: Implications of temperature-dependent thermal diffusivity and rheology: *Journal of Geophysical Research*, v. 115, B12417, doi:10.1029/2010JB007727.

Nascimento, D.B., Ribeiro, A., Trouw, R.A.J., Schmitt, R.S., Passchier, C.W. 2016. Stratigraphy of the Neoproterozoic Damara Sequence in northwest Namibia: Slope to basin sub-marine mass-transport deposits and olistolith fields. *Precambrian Research* 278, 108-125.

Nascimento, D.B., Schmitt, R.S., Ribeiro, A., Trouw, R.A.J., Passchier, C.W. and Basei, M.A.S. 2017. Depositional ages and provenance of the Neoproterozoic Damara Supergroup (northwest Namibia): Implications for the Angola–Congo and Kalahari cratons connection. *Gondwana Research*, **52**, 153–171, https://doi. org/10.1016/j.gr.2017.09.006

Nelson, K.D., Zhao, W., Brown, L.D., Kuo, J., Che, J., Liu, X., Klemperer, S.L., Makovsky, Y., Meissner, R., Mechie, J., Kind, R., Wenzel, F., Ni, J., Nabelek, J., Leshou, C., Tan, H., Wei, W., Jones, A.G., Booker, J., Unsworth, M., Kidd, W.S.F., Hauck, M., Alsdorf, D., Ross, A., Cogan, M., Wu, C., Sandvol, E., and Edwards, M., 1996, Partially molten middle crust beneath southern Tibet: A synthesis of Project INDEPTH results: *Science*, v. 274, p. 1684–1688, doi:10.1126 /science.274.5293.1684.

Oliver, G.J.H., 1994. Mid-crustal detachment and domes in the central zone of the Damara orogen Namibia. Journal of African Earth Science. **19**, 331–344.

Oliver, G.J.H., 1995. The central zone of the Damara Orogen, Namibia as a deep metamorphic core complex. Commun. Geol.Survey Namibia **10**, 33–41.

Oliver, G.J.H. and Kinnaird, J.A. 1996. The Rossing SJ Dome, Central Zone, Damara Belt, Namibia: an example of mid-crustal extensional ramping. *Commun. Geol. Surv. Namibia*, 1996, 11, 53–64.

Ormond, R. J., J. Lehmann, P. Hasalová, and M. Elburg. 2024. Migmatite Dome as a Result of Multi-Fold Interference Pattern, in the Damara Belt, Namibia. *Journal of Structural Geology 180: 105059.*

Ostendorf, J., Jung, S., Berndt-Gerdes, J., Hauff, F., 2014. Syn-orogenic high-temperature crustal melting: Geochronological and Nd–Sr–Pb isotope constraints from basement-derived granites (Central Damara Orogen, Namibia). *Lithos* **192**, 21–38.

Osterhus, L., Jung, S., Berndt, J., Hauff, F., 2014. Geochronology, geochemistry and Nd, Sr and Pb isotopes of syn-orogenic granodiorites and granites (Damara orogen, Namibia)—arc-related plutonism or melting of mafic crustal sources? *Lithos* **200–201**, 386–401.

Passchier C.W., Trouw R., Schmitt R.S. (2016) How to make a transverse triple junction—new evidence for the assemblage of Gondwana along the Kaoko-Damara belts, Namibia. *Geology 44(10):843– 846.* https://doi.org/10.1130/G38015.1

Paul, A., Jung, S., Romer, R.L., Stracke, A. and Hauff, F., 2014. Petrogenesis of synorogenic high-temperature leucogranites (Damara orogen, Namibia): Constraints from U–Pb monazite ages and Nd, Sr and Pb isotopes. *Gondwana Research*, 25(4), pp.1614–1626.

Poli, L.C. 1997. Mid-crustal geodynamics of the southern Central Zone, Damara Orogen, Namibia. Unpublished PhD thesis, University of St Andrews, Scotland. http://hdl.handle.net/10023/15573

Poli, L.C., Oliver, G.J.H., 2001. Constrictional deformation in the Central Zone of the Damara Orogen Namibia. *Journal of African Earth Science*. 33, 303–312.

Ramsay, J. G., 1962. Interference patterns produced by the superposition of folds of similar type. *The Journal of Geology, 466–481. 27*

Rosenberg, C.L., Handy, M.R., 2005. Experimental deformation of partially melted granite revisited: implications for the continental crust. *Journal of Metamorphic Geology*. **23**, 19–28.

Rowe CD, Fagereng A, Miller JA, Mapani B. 2012a. Signature of coseismic decarbonation in dolomitic fault rocks of the Naukluft Thrust, Namibia. *Earth Planet. Sci. Lett*. 333:200–10

Royden, L.H., Burchfiel, B.C., van der Hilst, R.D., 2008. The geological evolution of the Tibetan Plateau. *Science 321, 1054–1058.*

Sawyer, E.W., 1979. The geology of an area south-east of Walvis Bay: Lithology and field relationships. *Rep. geol. Surv. S.W. Afr. (unpublished).*

Searle, M.P., Godin, L., 2003. The South Tibetan Detachment system and the Manaslu leucogranite: a structural re-interpretation and restoration of the Annapurna–Manaslu Himalaya, Nepal. *Journal of Geology* 111, 505 – 523.

Searle, M.P., Cottle, J.M., Streule, M.J. & Waters, D.J. 2009. Crustal melt granites and migmatites along the Himalaya: melt source, segregation, transport and granite emplacement mechanisms. *Transactions of the Royal Society of Edinburgh*, **100**, 219–233, doi:10.1017/S175569100901617X.

Simon, I., Jung, S., Romer, R.L., Garbe-Schonberg, D., Berndt, J., 2017. Geochemical and Nd-Sr-Pb isotope characteristics of synorogenic lower crust-derived granitoids (Central Damara orogen, Namibia). *Lithos* **274–275**, 397–411.

Simony, P.S., and Carr, S.D., 2011, Cretaceous to Eocene evolution of the southeastern Canadian Cordillera: Con tinuity of Rocky Mountain thrust systems with zones of "in-sequence" mid-crustal flow: *Journal of Structural Geology*, v. 33, p. 1417–1434, doi:10.1016/j.jsg .2011.06.001.

Smith, D.A.M., 1965. The geology of the area around the Khan and Swakop Rivers in SW Africa. *Geological Survey South Africa, Memoir 3*, 1-113.

Steck, A., 2008, Tectonics of the Simplon massif and Lepontine gneiss dome: Deformation structures due to collision between the underthrusting European plate and the Adriatic indenter: *Swiss Journal of Geosciences*, v. 101, p. 515–546, doi:10.1007/s00015-008-1283-z.

Tack, L., Williams, I. and Bowden, P., 2002. SHRIMP constraints on early post-collisional granitoids of the Ida Dome, central Damara (Pan-African) Belt, western Namibia. *Abstracts of the 11th IAGOD Quadrennial Symposium and Geocongress, Windhoek, Namibia*

Toé, W., Vanderhaeghe, O., André-Mayer, A.-S., Feybesse, J.-L., & Milési, J.-P. (2013). From migmatites to granites in the Pan-African Damara orogenic belt, Namibia. *Journal of African Earth Sciences*, **85**, 62–74. https://doi.org/10.1016/j.jafrearsci.2013.04.009

Unsworth, M.J., Jones, A.G., Wei, W., Marquis, G., Gokarn, S.G., Spratt, J.E., and the INDEPTH-MT Team, 2005, Crustal rheology of the Himalaya and southern Tibet inferred from magnetotelluric data: *Nature*, v. 438, p. 78–81, doi:10.1038/nature04154.

Wang, S., Jiang, Y.D., Weinberg, R., Schulmann, K., Zhang, J., Li, P.F., Xiao, M., Xia, X.P., 2021.Flow of Devonian anatectic crust in the accretionary Altai Orogenic Belt, central Asia: insights into horizontal and vertical magma transfer. *Geological Society of America Bulletin*. **23**. https://doi.org/10.1130/B35645.1.

Ward, R.A., Stevens, G. and Kisters, A.F.M., 2008. Fluid and deformation induced partial melting and melt volumes in low-temperature granulite-facies metasediments, Damara Belt, Namibia. *Lithos*, 105, pp.253–271.

Westbrook, G.K., Ladd, J.W., Buhl, P., Bangs, N., and Tilley, G.J., 1988, Cross-section of an accretionary wedge: Barbados Ridge complex: *Geology*, v. 16, p. 631–635, doi: 10.1130/0091-7613(1988)0162.3 .CO;2.

Willett, S.D., Beaumont, C., and Fullsack, P., 1993, Mechanical model for the tectonics of doubly vergent compressional orogens: *Geology*, v. 21, p. 371–374, doi: 10.1130/0091-7613(1993)0212.3 .CO;2.